Journal of Structural Geology 140 (2020) 104156

Contents lists available at ScienceDirect

Journal of Structural Geology

journal homepage: http://www.elsevier.com/locate/jsg

Mineral precipitation as a mechanism of fault core growth

Owen A. Callahan [a,1,*], Peter Eichhubl [a], Nicholas C. Davatzes [b]

[a] Bureau of Economic Geology, Jackson School of Geosciences, The University of Texas at Austin, 10100 Burnet Rd, Bld 130, E0630, Austin, TX 78758-4445, USA
[b] Department of Earth and Environmental Science, Temple University, 326 Beury Hall, 1901 N. 13th Street, Philadelphia, PA 19122, USA

ARTICLE INFO

Keywords:
Alteration
Silicification
Fault evolution
Fault architecture
Dixie Valley

ABSTRACT

Faults vary in structural style, from simple planes to complex systems composed of fault cores and damage zones. Increased fault complexity results from the interaction of mechanical and chemical processes, including fracture growth, shear, and linkage, and mineral dissolution and precipitation. Although water-rock interaction is traditionally associated with fault rock weakening and shear localization, we investigate processes of fault core widening by water-rock interactions that resulted in quartz precipitation. We combine field and petrographic observations with prior mechanical characterization to assess the impact of alteration and cementation on fault architecture at the Dixie Comstock epithermal gold deposit, Nevada, USA. Mineralized portions of the fault contain strong, thick, silicified fault cores and wide, weak damage zones, with evidence for widening of the core through entrainment of damage zone material and repeated cycles of embrittlement, dilation, and cementation. We present a model of fault zone evolution in which the hydrothermal regimes favoring either alteration-weakening or precipitation-strengthening result in distinct fault zone architecture and mechanical and flow properties of fault systems. Alteration-weakening favors localization of the fault into thinner, clay-rich, low permeability fault cores. Precipitation-strengthening promotes thick, strong, and low permeability fault cores, with mineralization-embrittlement enhancing transient permeability following coseismic failure.

1. Introduction

Fault-fracture networks vary from single planes to complex core and damage zones. The term fault core describes the innermost high-strain part of fault zones that is structurally, texturally, mechanically, and frequently compositionally distinct from the outer and less deformed damage zone which transitions into the undeformed host formation. The fault core is commonly composed of variably cohesive fault rock, including gouge or cataclasite and breccia, and bound or cut by one or multiple slip surfaces (Sibson, 1977; Chester and Logan, 1986; Caine et al., 1996; Jefferies et al., 2006; Woodcock and Mort, 2008; McKay et al., 2019). Compared to the fault core, fault damage zones contain lesser amounts of fragmented, pulverized, or chemically altered rock but, compared to the host formation, an increased abundance of opening-mode and sheared fractures, veins, or deformation bands (Davatzes et al., 2003; Kim et al., 2004; Sutherland et al., 2012; Choi et al., 2016; Peacock et al., 2017; Ostermeijer et al., 2020). Caine et al. (1996) presented a classification of fault zone hydrology based on properties of the fault core and damage zones that included localized conduit, distributed conduit, localized barrier, and dual conduit-barrier endmembers. Building in part on this classification, the importance of relative thickness, geometric distribution, and physical properties of fault cores versus damage zones now has well-documented implications for the coupled hydrologic and mechanical behavior of faults (Evans et al., 1997; Rowland and Sibson, 2004; Cox, 2005; Wibberley et al., 2008; Eichhubl et al., 2009; Caine et al., 2010; Faulkner et al., 2010; Gratier, 2011; Morton et al., 2012; Bense et al., 2013). Thus, characterizing the processes that contribute to diverse fault zone architecture in the subsurface may improve our understanding of a variety of geoscience topics of particular relevance to society, from the geometry of fault-controlled mineral and hydrothermal resources, to the quality of fault-traps in oil, gas, and CO_2 sequestration reservoirs, and the seismogenic behavior of active faults.

Various mechanisms are employed to explain the development of fault zone architecture, with two primary conceptual models emphasizing 1) the evolutionary character of fault zones from precursor structures and 2) frictional-wear processes during fault slip. Linkage and the formation of subsidiary faults at segment boundaries exert a

* Corresponding author.
E-mail address: ocallahan@utexas.edu (O.A. Callahan).
[1] Present address: Department of Geography, Texas State University, Evans Liberal Arts, 601 University Drive, San Marcos, TX, 78640

https://doi.org/10.1016/j.jsg.2020.104156
Received 6 March 2020; Received in revised form 2 August 2020; Accepted 6 August 2020
Available online 16 August 2020

principal control on fault zone thickness in precursor-type models (e.g. Childs et al. (1996); Crider and Peacock (2004); Davatzes et al. (2003); Myers and Aydin (2004)). In these models, fault formation and megascopic geometry is influenced by inherited and precursor fabrics and structures, with the fault eventually becoming localized on favorable and/or newly formed features within a broader deformed region. Frictional-wear models emphasize the contribution of accumulated slip on fault zone thickness, which grows as asperities break, wear, and smooth (Scholz, 1987; Hull, 1988; Watterson et al., 1998; Brodsky et al., 2011; Lyakhovsky et al., 2014). In addition, various authors have described the accumulation of fault zone damage and fault zone thickening based on migrating or interacting process zones at fault tips (Shipton and Cowie, 2001; Mitchell and Faulkner, 2009; Savage and Brodsky, 2011). Multiple elements from *both* conceptual fault zone models, emphasizing either precursor structures or frictional-wear, likely contribute to the architectural evolution of fault zones (Childs et al., 2009). However, the conceptual framing of fault zone evolution frequently emphasizes one model or mechanism over another, which may confound subsequent interpretations (Scibek et al., 2016; Shipton et al., 2019). For instance, both models commonly assume quasi-static or monotonic changes in mechanical properties, without explicitly addressing localized and diverse changes in rock properties resulting from fault-controlled chemical fluid-rock interaction (Dewhurst and Jones, 2003).

Increasingly, the role of fluids and fluid-rock interactions in fault zones, with resulting changes to hydrologic and mechanical properties, are considered contributing factors in fault zone behavior. Common fluid-rock interactions and resulting mineralogical and textural alteration are associated with fault-rock weakening in laboratory tests (Sleep and Blanpied, 1992; Blanpied et al., 1995, 1998 Escartin et al., 2001; Collettini et al., 2009; Ikari et al., 2011; Lockner et al., 2011) and implicated in the localization of fault-zone deformation in field-structural investigations (Chester and Logan, 1986; Blenkinsop and Sibson, 1992; Chester et al., 1993; Bruhn et al., 1994; Schulz and Evans, 1998; Jefferies et al., 2006; Solum et al., 2010; Bradbury et al., 2014; Niwa et al., 2015; Backeberg et al., 2016; Yang et al., 2018). These investigations show that progressive damage resulting in grain size reduction and alteration of primary minerals to weaker phyllosilicate minerals, such as serpentinite, chlorite, or clays, can result in reduced fault strength, and is referred to as alteration-weakening or reaction-softening. Alteration-weakening has garnered considerable attention as a possible factor influencing fault creep on segments of seismogenic faults (Blenkinsop and Sibson, 1992; Wintsch et al., 1995; Moore et al., 1996; Rutter et al., 2001; Lockner et al., 2011; Barth et al., 2013; Moore and Lockner, 2013; Bradbury et al., 2014).

Similarly, fluid-rock interactions and mineral precipitation have long been recognized as essential processes in the generation of fault-hosted ore deposits (e.g. Lindgren (1913)). In many world-class systems, mineral precipitation is extensive. For instance, excavations in the Martha Hill gold-silver deposit in New Zealand revealed quartz veins that were >10 m thick (Spörli and Cargill, 2011), and the Mother Lode gold deposits in California contain arrays of mineralized veins that extend along strike for 10s of kilometers with ore grades extending down dip more than 2 km (Becker and Ransome, 1928; Sibson, 2020). Cycles of faulting, fracturing, fluid flow, and mineralization inferred from gold-quartz mineral deposits like the Mother Lode system contributed to the Sibson et al. (1988) "fault-valve" model.

Well-cemented faults may be less common than faults with weak, clay-rich cores, but they are nevertheless important features in geothermal reservoirs and mineral deposits, are observed in a variety of tectonic settings, and are associated with measurable changes in fault zone structures. Moore and Saffer (2001) noted that quartz veins and quartz cementation become dominant features in subduction zone mélange at temperatures over 200 °C, and Moore and Byrne (1987) suggested that mélange may thicken due in part to this low-grade metamorphism and the resultant strengthening. Faulkner et al. (2008)

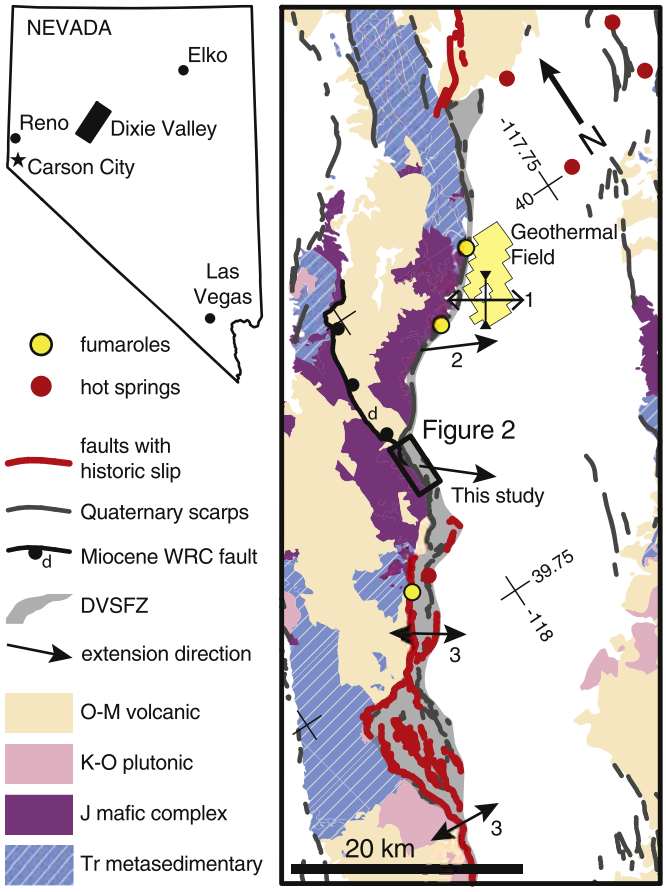

Fig. 1. Regional map showing the location of Dixie Valley (black rectangle, inset) and the Dixie Comstock epithermal deposit (black box). The epithermal deposit is hosted in a north-striking, east-dipping segment of the Dixie Valley - Stillwater Fault Zone (DVSFZ), between fault segments with historic slip and active hydrothermal features. Fault orientation is partially controlled by the Miocene White Rock Canyon (WRC) Fault. Modern stress orientations (1; Hickman et al. (2007)) are consistent with SE-NW extension indicated by fault striations (2) and SE-NW to E-W extension associated with the 1954 Dixie Valley earthquake (3) (Caskey et al., 1996; Caine, 1999).

speculated that cementation may contribute to wide faults in crystalline rocks where weakening would otherwise favor localization. And Laubach et al. (2014), Williams et al. (2017), and Ferraro et al. (2019) describe the impact of differential diagenetic cementation on fault zone architecture and evolution in siliciclastic and carbonate rocks. These field-based observations of fault zone cements and fault properties are particularly compelling because experimental and numerical investigations have shown that inclusion of mineral precipitation or fault rock healing better replicates fault slip behavior in some settings (Karner et al., 1997; Cowie, 1998; Olsen et al., 1998; Muhuri et al., 2003; Tenthorey et al., 2003; Yasuhara, 2005; Chen et al., 2015). Yet the impact of mineral precipitation and fault rock strengthening on fault zone evolution tends to be overlooked in fault zone models that traditionally emphasize structural or mechanical aspects of fault zone evolution.

In this study, we examine how fluid-rock interactions resulting in alteration and mineral precipitation impacted fault zone architecture and fault zone evolution in a well-exposed normal fault system at the Dixie Comstock epithermal deposit, Dixie Valley, Nevada, USA (Fig. 1). We hypothesize that hydrothermal alteration and precipitation result in fundamental changes in mechanical properties of fault rocks, and that these changes contribute to, not just arise from, wide fault cores commonly encountered in mineralizing epithermal and porphyry environments (Simmons et al., 2005; Micklethwaite, 2009; Jensen et al., 2019). We test this hypothesis by correlating spatial variations in fault

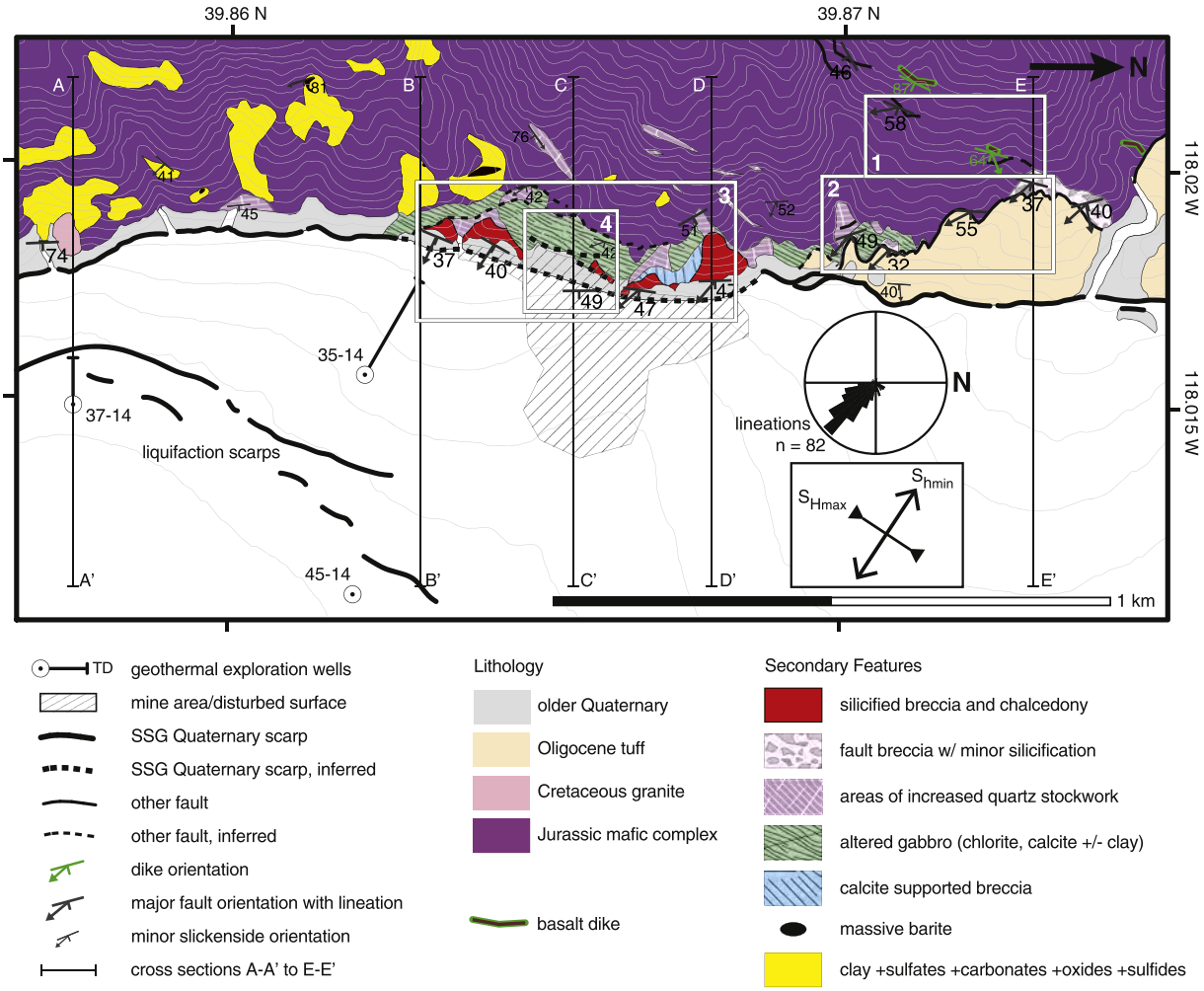

Fig. 2. Geologic map of the Dixie Comstock epithermal deposit. Silicification and mineralization overprints a larger region of damaged and chlorite, calcite ±clay altered gabbro. Rose diagram shows fault lineations with a mean trend ~130°, similar to the extension direction in Dixie Valley and S_{hmin} (inset) measured in wells in the producing geothermal field approximately 15 km to the northeast (Hickman et al., 2007). Carbonate, barite, sulfide, oxide, and clay alteration is associated with Cretaceous plutons. Background alteration in the Jurassic Humboldt Igneous Complex (Jgb in later figures) is not differentiated but includes widespread chlorite, albite, and calcite alteration. Numbered boxes correspond to fault areas described in the text. Cross sections AA′ to EE′ are shown in Fig. 3. Modified in part from Vikre (1993).

zone architecture and fault core elements with prior petrographic, mineralogic, and mechanical characterization (Callahan et al., 2019, 2020). We document evidence for the growth of the fault core by silicification, embrittlement, and dilation as well as through incorporation of previously altered and damaged footwall material. Based on our observations and using a space-for-time substitution, we present an expanded conceptual model of fault zone evolution that explicitly includes the impact of hydrothermal regime, and the tendency toward fault rock weakening or strengthening, on fault zone architecture.

2. Geologic Setting

2.1. Dixie Valley – Stillwater Fault Zone

The Dixie Valley – Stillwater Fault Zone is a seismically active, segmented normal fault system located in northwestern Nevada, U.S.A., which juxtaposes Mesozoic sedimentary, metamorphic, and igneous units and Cenozoic volcanic units against Quaternary basin fill (Fig. 1). The fault zone is generally northeast trending, with significant changes in orientation associated with reactivation of north-south striking Miocene normal faults (Parry et al., 1991) and with changes in lithology (Caskey et al., 1996). Based on fault scarp orientations and displacement associated with the 1954 Fairview Peak-Dixie Valley earthquake sequence (M 7.2 and ~6.8), the modern extension direction in the southern Dixie Valley-Stillwater Fault Zone is estimated to be 94 ±15° (Whitten, 1957; Caskey et al., 1996) and 124–125° in central Dixie Valley (Thompson and Burke, 1973; Caskey et al., 1996). This is consistent with longer-term extension directions of 116–140° based on striations on exhumed portions of the fault (Thompson and Burke, 1973; Okaya and Thompson, 1985; Caine, 1999) and the orientation of minimum horizontal principal stress in the Dixie Valley geothermal field, 123–160° (Hickman et al., 1998, 2007). Normal, dip-slip displacement in northern Dixie Valley is roughly 3 km in the last 8 m.y. (Okaya and Thompson, 1985; Carena and Friedrich, 2018), with as much as 6 km of post-Oligocene displacement in southern Dixie Valley (Thompson et al., 1967; Parry and Bruhn, 1990).

Exhumed portions of the Dixie Valley – Stillwater Fault Zone have been the loci of extensive research on fault zone architecture (Power and Tullis, 1989; Parry et al., 1991; Zhang et al., 1991, 1999; Bruhn et al., 1994; Caine et al., 1996; Caine, 1999; Caine et al., 2010; Candela and Renard, 2012) as well as fault and fault rock mechanics (Power and Tullis, 1992; Seront et al., 1998; Hickman et al., 2007; Candela et al., 2011; Callahan et al., 2019, 2020) in the context of hydrothermal processes. Regional hydrothermal alteration in the footwall includes sodic

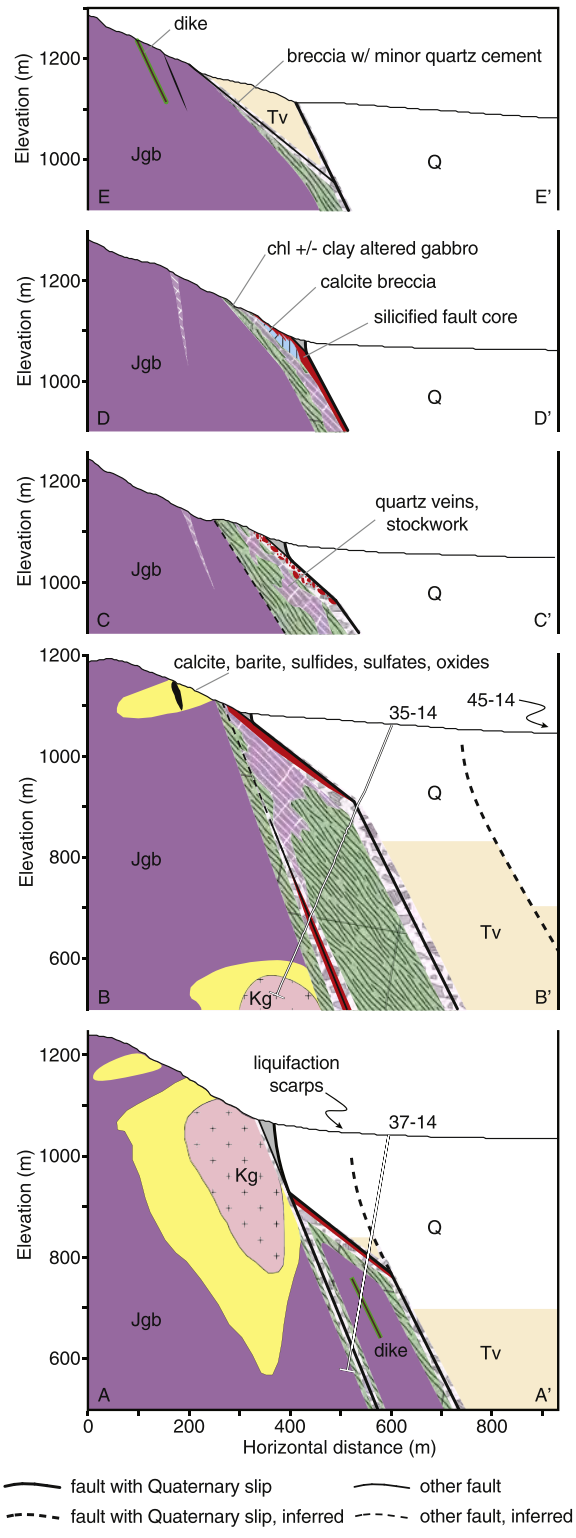

Fig. 3. Serial cross sections from south to north, AA′ to EE′, from Fig. 2. Increased hydrothermal alteration and economic mineralization, widening of the fault zone and associated damage, and a thicker cemented fault core occur in sections BB′ to DD'. Well bore trajectories, and lithologic and fault contact interpretations for 37–14 and 35–14 provided by Robin Zuza, Ormat Technologies, Inc. Legend after Fig. 2.

and calcic metasomatism of Jurassic mafic rocks (Dilek and Moores, 1995; Johnson and Barton, 2000) and potassic and sericitic alteration of Oligocene plutons (Parry et al., 1991; John, 1995). Localized, fault-controlled sericite, chlorite-carbonate-hematite, chlorite-talc, quartz-kaolinite, smectite, zeolite, and silicic assemblages are described in discrete segments of the fault system (Power and Tullis, 1989; Parry et al., 1991; Vikre, 1993; Bruhn et al., 1994; Hickman et al., 2000; Kennedy-Bowdoin et al., 2004; Caine et al., 2010; Schwering, 2013; Callahan et al., 2019). Modern hydrothermal features include the Dixie Valley geothermal field, which generates ~56 MWe from a ~248 °C fault and fracture reservoir at 2.5–3 km depth (Benoit, 1992; Blackwell et al., 2000, 2007), as well as fault-related fumaroles, hot springs, sinter, and travertine deposits (Fig. 1) (Lutz and Hulen, 2000; Lutz et al., 2002).

2.2. *Faulting, alteration, and mineralization at the Dixie Comstock epithermal gold deposit*

The Dixie Comstock epithermal gold deposit is located on a north-striking, east-dipping segment of the Dixie Valley – Stillwater Fault Zone. Fault orientation is partially controlled by interaction with the north-striking, Miocene-age White Rock Canyon Fault that transects the Stillwater Range and places Oligocene volcaniclastics against Jurassic mafic plutonic and volcanic rocks of the Humboldt Igneous Complex (Jgb) (Figs. 1 and 2). The deposit was discovered in 1934 and was mined intermittently from 1938 to 1970 (Vanderburg, 1940; Wilden and Speed, 1974; Vikre, 1993). Total yield was approximately 4600–5000 oz of gold from 10,000–17,000 tons of altered gabbro, quartz stockwork, silicified fault rocks, and low-grade hanging wall alluvium (Wilden and Speed, 1974; Vikre, 1993). Drilling between 1982 and 1984 defined an additional 1.8 million tons of ore at 0.058 oz/ton in a 5–30 m thick fault zone "mullion" (Vikre, 1993).

The Jurassic Humboldt Igneous Complex is a tectonically imbricated mafic volcanic-arc complex composed of coeval intrusive units, from anorthosite to monzonite, basaltic to andesitic dikes, and volcanics units ranging from basalt to dacite (Wilden and Speed, 1974; Dilek and Moores, 1995). Hornblende K–Ar and $^{40}Ar/^{39}Ar$ ages are mid-Jurassic (170 ±2 Ma), with younger biotite ages reflecting Cretaceous and Cenozoic magmatism and exhumation (Kistler and Speed, 2000). Lithologies in the immediate vicinity of Dixie Comstock include fine to coarse grained plagioclase- and pyroxene-rich hornblende gabbro, anorthosite, and basalt (Wilden and Speed, 1974; Speed, 1976; Vikre, 1993). Small bodies of pink, fine grained granite intrude the Humboldt Igneous Complex in the southern part of the map area (Figs. 2 and 3). K–Ar ages from albite associated with the granite intrusions are 93.2 ±7.8 Ma (Vikre, 1993). Unaltered, steeply east-dipping dikes in the northern part of the map area are tentatively correlated with regionally extensive 13–17 Ma basalt flows (Nosker, 1981; Gonsior and Dilles, 2008).

Early phases of normal faulting and fault-related alteration at Dixie Comstock, recorded by 15 ±0.5 to 11.1 ±0.3 Ma K–Ar sericite ages of sericitized fault rock (Vikre, 1993), correspond with Miocene volcanism and a regional shift in extension direction from E-W to NW-SE around 13-10 Ma (Zoback et al., 1981; Hudson and Geissman, 1991; Parry et al., 1991). Continued fault activity into the Quaternary is represented by 2.0–2.5 ka scarps with 3–5 m of throw that cut Quaternary colluvial, alluvial, and lacustrine deposits in the southern part of the map area and Quaternary and Oligocene units north of the mine (Fig. 2) (Thompson and Burke, 1973; Wallace and Whitney, 1984; Bell et al., 2004; Caskey and Ramelli, 2004). Faults in colluvium exposed by mine workings reveal down-to-the-east dip slip, however Quaternary scarps through the middle of the field site are obscured by past mining activity.

Regional sodic and calcic alteration of the Jurassic Humboldt Igneous Complex (Dilek and Moores, 1995; Johnson and Barton, 2000) manifests as chlorite, calcite, and albite ±epidote replacing plagioclase and mafic minerals, and calcite-hematite ±quartz and cataclasite veins (Table 1, Fig. 4). Background alteration in the southern part of the map

Table 1
Mineralogy of representative alteration assemblages in different fault settings at dixie comstock from X-Ray Diffraction.

Fault Setting	Area	Alteration Minerals	Sample[a]	Cor spike[b] (wt%)	Cor (wt%)	Normalized wt%							
						quartz	feldspars	amphiboles and pyroxenes	calcite	epidote	chlorite	sericite	clays	oxides + sulfides
footwall gabbro	2	minor chl, alb	083114-2A	10.2%	9	10	76		1	2	8	2		2
footwall gabbro	2	minor chl, alb	083114-2B	10.0%	9	10	77			1	7	3		2
damage zone	–	chl, minor cal, alb	083114-1C	10.0%	11	2	56	16	2	3	20		1	
damage zone	3, 4	chl, minor cal, alb	061214-5	10.0%	11	11	38	16	2	2	29		2	
damage zone	3, 4	chl, minor cal, alb	052815-3B	10.0%	9	2	59		1	1	32	4		
damage zone	3, 4	chl-cal, alb	052815-3A	10.2%	9	1	57		19		22			1
silicified fault core	3	silicified, cal	090114-5C	10.1%	8	55	2		41		2			
silicified fault core	3	silicified	090114-5B	10.0%	8	88	5		4		4			1
silicified fault core	3	silicified	061114-4B	10.0%	7	91	5				4			1
silicified fault core	3	silicified	052815–2	10.0%	6	97			1		3			1

[a] Sample locations are shown on supplemental Map S1.
[b] Corundum spike. XRD methods described in Callahan et al. (2019).

area is overprinted by large masses (>10 m) of barite, calcite, and pyrite as well as regions of quartz, albite, sericite, kaolinite, and iron oxide alteration around and possibly above small bodies Cretaceous granite (Vikre, 1993) (Figs. 2 and 3). Within the mine area, sodic and calcic alteration is cut by quartz stockwork veins and overprinted and entrained in silicified fault breccia (Table 1, Fig. 5). Late calcite mineralization occurs as massive calcite-supported breccia, as rhombic crystals in quartz-lined fractures, and as blades in vugs in cockade breccia. The occurrence of bladed calcite (Callahan et al., 2019) and liquid- and vapor-rich inclusions in quartz veins with homogenization temperatures between 160 and 180 °C (Vikre, 1993) are consistent with mineralization in a shallow, boiling, epithermal environment. Vikre (1993) proposed a mid-Pleistocene age for epithermal mineralization based on minor silicification of Pleistocene Lake Dixie gravels and U–Pb calcite ages >0.35 Ma. MacNamee et al. (2015) reported 0.3 ±0.2 Ma and 0.9 ±0.4 Ma apatite (U–Th)/He cooling ages north of Dixie Comstock, in reasonable agreement with Vikre's (1993) suggested age.

3. Field observations of fault zones at Dixie Comstock

Megascopic fault zone geometry, fault zone architecture, and hydrothermal alteration vary along strike north and south of the Dixie Comstock deposit. Mineralization is located in a right-stepping, hard-linked extensional fault relay between subparallel fault segments with normal-oblique, right-lateral displacement across a 10–30° change in fault strike (Figs. 2 and 3). North of the mine, polished and partially cemented slicken surfaces strike ~000° and dip 43–55° east. In the southern part of the mine area prominent triangular facets armored by silicified fault breccia strike ~025° and dip 28–52° southeast. The range front south of the mine again strikes ~ N–S, but the fault is poorly exposed due to erosion of altered rock and onlap of lacustrine shoreline deposits. Extension direction across the field area based on striations on silicified fault rocks, on mineralized fracture surfaces, and in unmineralized gouge is 133 ±7° (see Supplemental Table S1).

The observation that exhumed fault cores, the volume of rock that records a discrete increase in shear strain reflected in the accumulation of gouge, cataclasite, and chaotic breccia, varies in thickness and degree of preservation in different segments of the fault prompted our examination of the relationship between the type and intensity of alteration and fault zone architecture. Below we describe differences in fault zone elements, particularly the thickness of the fault core as well as fractures and veins in the core and damage zone, and the type of alteration and

Fig. 4. Products of regional sodic and calcic alteration as well as preexisting fractures and cements in the Jurassic Humboldt Igneous Complex (Jgb) in the footwall at Dixie Comstock. All original photographs are archived in the supplemental data.

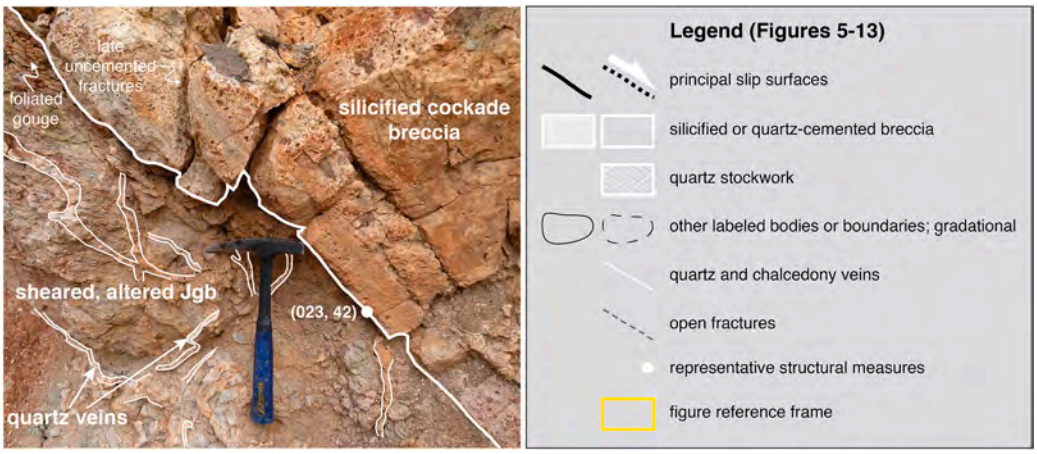

Fig. 5. Matrix-supported, quartz-cemented, and silicified fault breccia, Dixie Comstock epithermal deposit, including clasts of previously altered and damaged footwall gabbro (Jgb) as well as reworked quartz and chalcedony clasts. Quartz veins are cut by foliated gouge at the base of the silicified interval and offset by centimeter-scale slip within the footwall damage zone. Location shown in Fig. 8. Hammer for scale is 28 cm. Legend applies to Figs. 5–13.

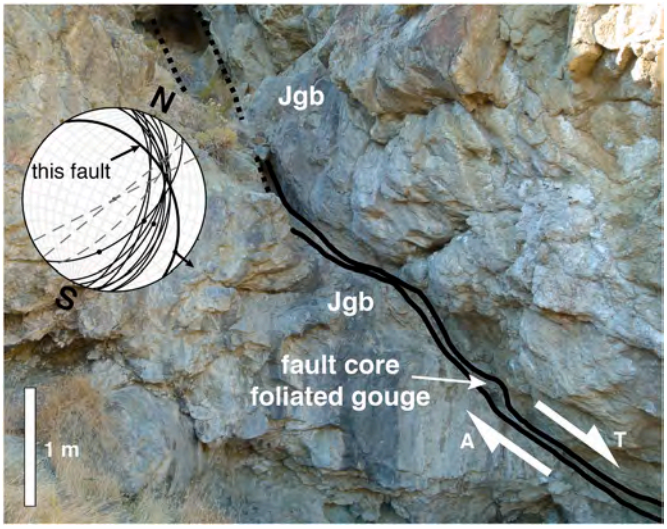

Fig. 6. Unmineralized fault in footwall gabbro from Area 1. Slip is localized in minor (~10 cm thick) foliated fault gouge and minor fault breccia. Undulations are enhanced by the oblique view. Stereonet shows orientations of small faults (solid), slickenlines (dots), and associated open fractures (dashed) in the northern part of the map area. See Fig. 5 for line and symbol explanations.

mineralization, at four distinct field areas, 1–4 in Fig. 2. From least to most structurally evolved, these are 1) small uncemented faults in sodic and calcic metasomatized and damaged gabbro in Area 1, 2) a body of moderately quartz-cemented breccia along the White Rock Canyon fault in Area 2, 3) the silicified and mineralized portion of the range front fault system in Area 3, and 4) disaggregated cemented fault breccia in Area 4. Georeferenced Map S1, with figure, sample, and scanline locations (Supplemental Table S2), is available as a .kmz file in the supplemental material.

3.1. Uncemented faults in Area 1

Area 1 is located 500 m north of the Dixie Comstock mine and 200–300 m west of the range front fault. This site exposes small, N- to NW-striking, moderately east-dipping normal faults (Fig. 2). These faults are traceable for tens of meters and, where they offset compositional variation in the gabbro, show less then ~5 m of normal displacement. Fault cores in this area consist of uncemented fault breccia and foliated fault gouge that is ~10 cm thick and bound by abrupt transitions into intact gabbro (Fig. 6). Striations within the fault gouge and decimeter-scale undulation at the core-wall rock transition indicate oblique normal right-lateral slip (Fig. 6, inset). Alteration in the wall rock adjacent to the fault core is consistent with regional sodic and calcic metasomatism. Fault-related damage is mostly limited to steeply-dipping uncemented opening-mode fractures in the hanging wall of some faults (Fig. 6, inset). The orientations of these faults and fractures are consistent with range front normal faulting in the stress state measured by Hickman et al. (2007).

3.2. Faults with minor quartz cement in Area 2

Area 2 is located 500 m north of the Dixie Comstock mine and 100–200 m west of the Quaternary range front fault, and exposes parts of the reactivated White Rock Canyon Fault (Fig. 2). The fault is broadly corrugated with a wavelength of hundreds of meters, and dips between 29 and 55° east. The fault core in the northern part of this area is poorly preserved, but where erosional relicts remain it contains meter-thick bodies of coarse, partially quartz-cemented breccia of gabbro clasts structurally above partially mineralized and oxidized slip surfaces on thin (10–50 cm) intervals of incohesive to cemented gouge and minimally altered plagioclase-rich gabbro (Fig. 7a and b). The southern White Rock Canyon Fault segment contains a 1–2 m thick fault core composed of a cohesive, partially quartz-cemented breccia of chloritized gabbro with multiple anastomosing slip surfaces, bound by less cohesive gouge and breccia at the base and well-developed slicken surfaces at the top (Fig. 7c). Basal slip is accommodated in a thin (<10 cm) interval of breccia and foliated gouge that separates the fault core from low angle quartz veins and mosaic breccia (after Woodcock and Mort (2008)) in the proximal fault damage zone (Fig. 7d, Table 1). Alteration mineralogy in the footwall gabbro resembles regional sodic and calcic assemblages (Table 1). Slickensides exposed on a >10 m wide exposure record oblique dextral normal slip and a late veneer of calcite-cemented clasts (Fig. 7e). 25–30 Ma Oligocene volcaniclastic units above the White Rock Canyon Fault segment are fractured and sheared, with rare antithetic, steeply NW dipping veins of hydrothermal quartz breccia, but hanging wall structures are not well-exposed. Based on the occurrence of these volcaniclastics in outcrop, which comprise a 1 km thick sequence in the interior of the Stillwater Range (Hudson and Geissman, 1991), total post-Oligocene vertical displacement is believed to be <1 km.

3.3. Silicified faults in Area 3

Area 3 includes the region adjacent to the Dixie Comstock mine, extending approximately 600 m along the range front and 200 m into

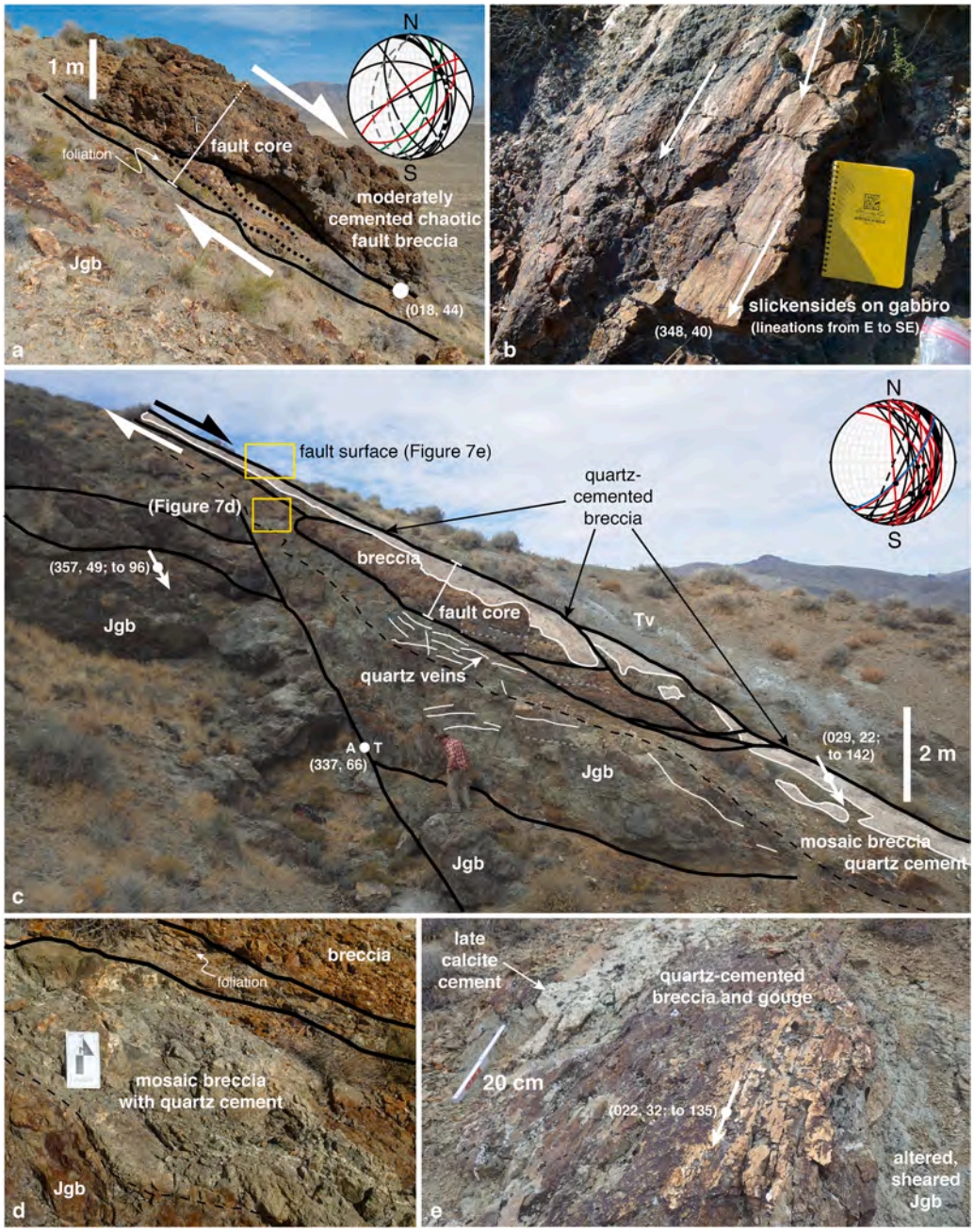

Fig. 7. Faults in Area 2 juxtaposing Oligocene volcanics against Humboldt Igneous Complex rocks (Jgb). Weak to moderate quartz cementation of cobble-sized gabbro clasts above intervals of incohesive breccia and gouge (a), as well as well-developed slickensides on thin, cemented intervals (b). Fault elements in the southern part of Area 2 (c, d, e). The fault core is composed of cohesive, partially quartz-cemented breccia of gabbro and Tertiary volcanics (?) with multiple anastomosing slip surfaces, bound by less cohesive gouge and breccia at the base and well-developed slicken surfaces at the top (e). Jgb in the footwall contains increased low angle, quartz-filled veins and mosaic breccia (c, d). Minor quartz veins, brecciation, and normal faulting is observed in the hanging wall volcanics (Tv) but are not well preserved. Yellow squares show locations of 7d and 7e. Symbols after Fig. 5. Stereonets show local faults (black lines), quartz veins (red lines), calcite veins (blue lines), basalt dikes (green lines), and fractures (dashed lines). (For interpretation of the references to color in this figure legend, the reader is referred to the Web version of this article.)

the footwall (Fig. 2). In this area, the dominant mineralized range front fault changes orientation: the northern part of the fault strikes north and dips moderately east at 40–55°, in the south, the fault strikes north-northeast with shallower 28–50° dips. Slicken fibers and striations document normal, dextral slip directed to 110–155°. Post-Oligocene vertical displacement, based on the occurrence of volcaniclastics in exploration wells (Fig. 3), is likely <1.5 km. Intense silicification of the range front fault (Table 1) produced prominent triangular facets extending ~300 m north and south of the mine, but these facets are not preserved in the footwall immediately adjacent to the mine (Area 4). The fault core exceeds 5 m in thickness in parts of the southern facets (Figs. 8 and 9), and is comprised of subparallel sheets of silicified fault breccias (see stereonets in Figs. 8 and 9), inverse graded breccia, cockade breccia, massive silica, and matrix supported blocks (<0.5 m wide) of variably altered gabbro clasts (Figs. 5 and 10). Repeated cycles of brecciation and cementation within the fault core are evident in outcrop and thin section (Figs. 10 and 11). The transition from the silicified fault core to altered damage zone is generally abrupt (Fig. 10a, f). However, 1–20 cm wide, quartz-cemented fractures extend from the fault core into and around blocks of altered and sheared footwall, completely surrounding this material in some areas (Figs. 1, 8 and 9b, d). These fractures include long (>10 m), steep, 1–20 cm wide, partially quartz, chalcedony, ±calcite-filled, east-west striking fractures as well as open, unmineralized fractures that strike subparallel to the range front and curve into a sheared interval at the base of the silicified blocks (Figs. 1, 8 and 9d, e, f). The interval below the silicified portion commonly contains several centimeters of foliated cataclasite and grades into course, oxidized, chlorite-calcite altered gabbro with multiple generations of cataclastic, quartz, and chalcedony veins (Fig. 10f). Locally intense areas of open, prismatic quartz-lined veins, graded quartz-supported breccias, chalcedony, quartz stockwork, and shearing associated with subsidiary faults extend >30 m into the footwall damage

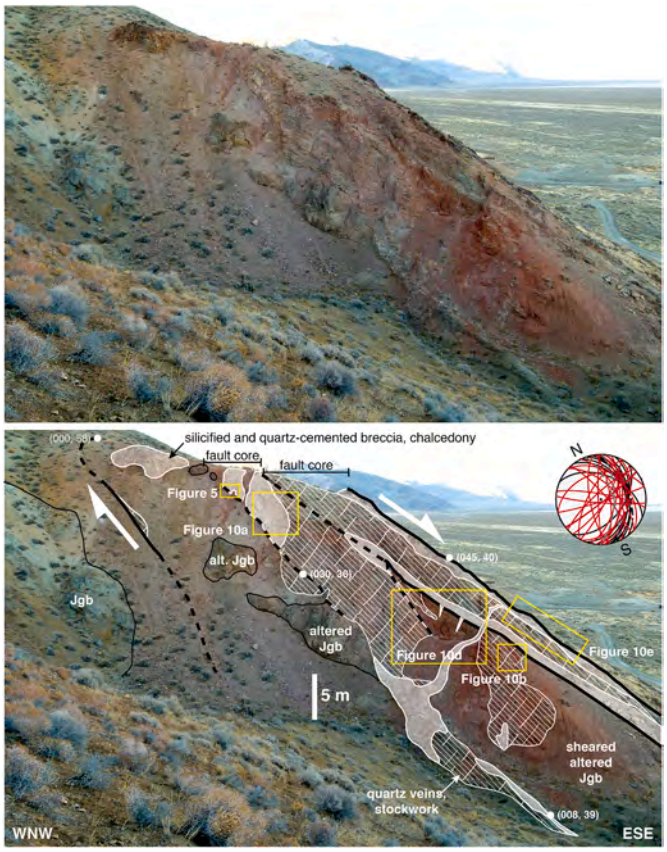

Fig. 8. Range front fault exposure in Area 3, south of the mine. Individual silicified fault breccias in this area exceed 3 m in thickness and the fault core is ~5 m thick. Extensive damage and quartz cementation extend >30 m into the footwall behind the range front fault. Blocks of fractured, moderately altered, quartz-cemented gabbro with complex fracture networks are located between and incorporated into matrix-supported, graded breccia, silicified fault breccia, and quartz stockwork veins. Heavy black lines in the stereonet show fault orientations; red lines show quartz vein orientations. We interpret interaction among multiple fault orientations, illustrated with structural measures on the principal slip surfaces, in this fault interval (Fig. 3, sections BB′ and CC′). (For interpretation of the references to color in this figure legend, the reader is referred to the Web version of this article.)

zone (Fig. 9). North of the mine, silicified triangular facets contain repeated layers of 10–50 cm thick, >5 m wide sheets of silicified fault breccia and chalcedony, and pods of graded breccia and chalcedony in cemented dilatant pinnate fractures (Fig. 12a), which also occur within the footwall damage zone (Fig. 12b). Clasts of silicified fault core with preserved slickensides within calcite supported breccia suggest instability and migration of the principal slip surface through time (Fig. 12c).

3.4. Disaggregated silicified fault core in Area 4

Area 4 is structurally most evolved and is located in the footwall of the range front fault in the immediate vicinity of the Dixie Comstock mine proper (Figs. 2 and 13a). For ~200 m along strike, the range front fault juxtaposes Quaternary deposits against a >10 m thick interval of clay-rich fault gouge and breccia containing large (>1 m) blocks of silicified fault breccia representing disaggregated portions of the former fault core and recording post-mineralization fault slip (Fig. 13b). Multiple oxide-coated slickensides occur throughout the clay-rich interval but deformation is most pronounced in clay-rich fault gouge in the main mine fault (Fig. 13a) suggesting renewed slip localization. Fault gouge is composed of montmorillonite, sericite, kaolinite, feldspar, and quartz (Vikre, 1993). Alteration minerals in the adjacent footwall include

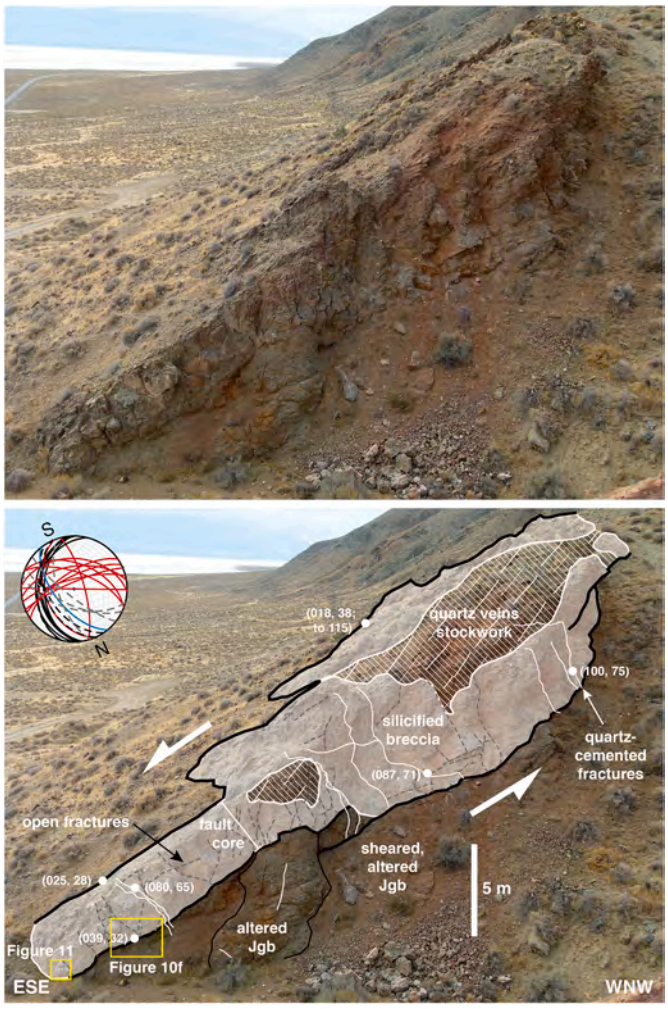

Fig. 9. Southern end of the silicified fault interval in Area 3 (looking south from Fig. 8). Thick (>3 m) section of silicified fault breccia incorporating blocks of altered footwall gabbro with undulatory basal shear zone (Fig. 10f) above weakly altered Jgb with multiple generations of quartz and cataclasite veins. The silicified interval contains open fractures that sole into the sheared interval, and steep ~ E-W striking quartz-filled fractures that cut into the basal shear zone. Black lines in the stereonet show fault orientations, red lines show quartz veins, blue lines are calcite veins, and dashed grey lines depict open fractures. See Fig. 5 for legend. (For interpretation of the references to color in this figure legend, the reader is referred to the Web version of this article.)

chlorite, calcite, hematite, sulfide, and clay in sheared gabbro (Table 1). The topography of the range front in this interval steps into the footwall, reflecting increased clay alteration in the footwall and degradation of the silicified facet.

4. Rock Mechanical Properties at Dixie Comstock

We previously reported results of rock and fracture mechanical testing of altered and damaged rock from Dixie Valley, including samples from Dixie Comstock (Callahan et al., 2019, 2020). Silicified fault core from Dixie Comstock exhibits a six-fold increase in unconfined compressive strength and fracture toughness, a tripling of Young's modulus, a two- to three-fold increase in shear modulus, and a halving of Poisson's ratio compared to footwall rocks with minor chloritization and calcification of plagioclase feldspar (Table 2). Mechanical testing was limited to samples that could be prepared as plugs and wafers, resulting in an underrepresentation of the weakest, clay-rich intervals, but reveals healed, silicified fault breccia is similar in strength and other mechanical

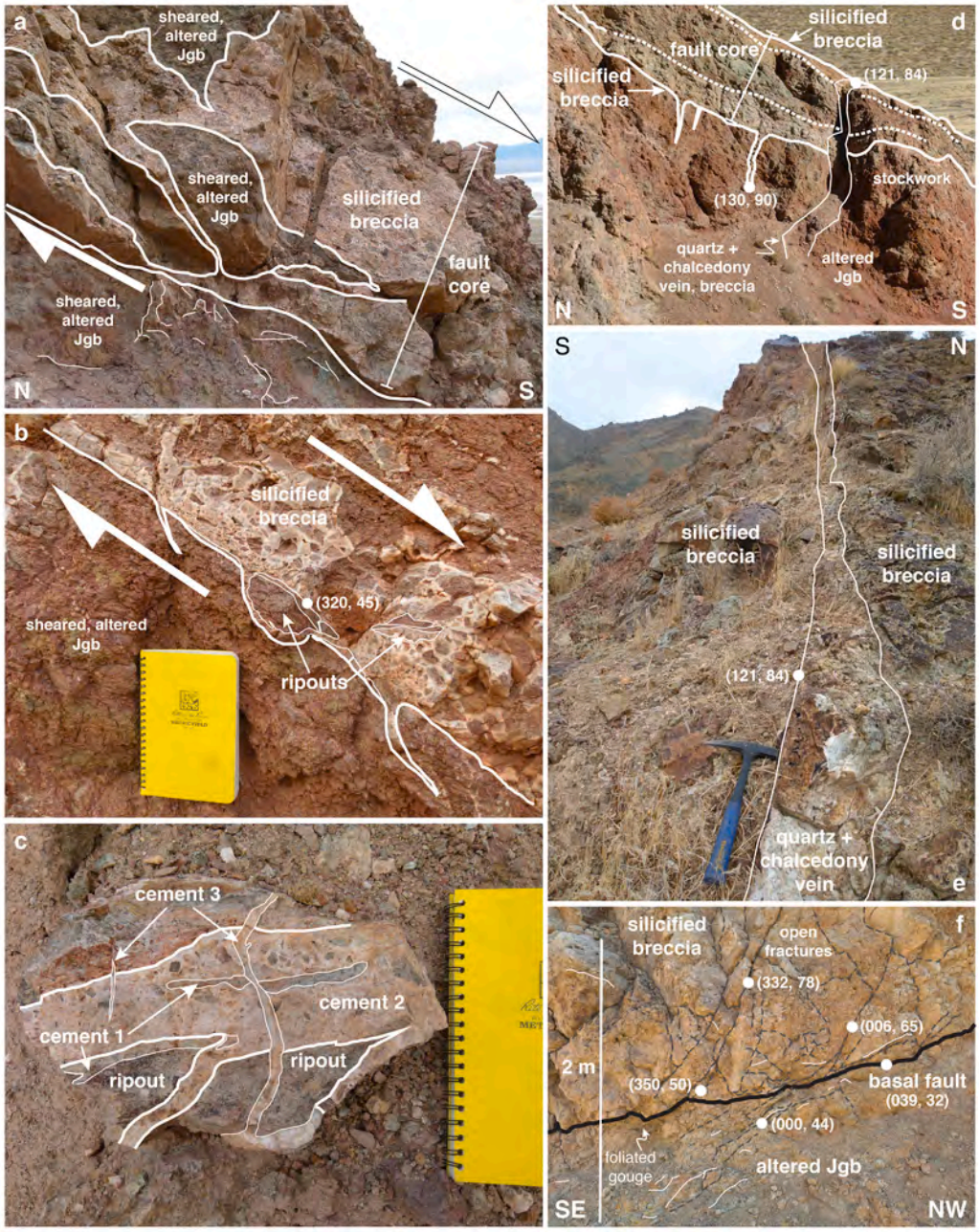

Fig. 10. Fault zone elements from Area 3 showing deformation in and around the silicified fault core. Widening of silicified fault breccia through incorporation of previously altered and damaged footwall (a–c). Steep, ~E-W striking, quartz, chalcedony, and uncemented fractures cut the silicified breccia and penetrate into the altered footwall rocks (d, e). Open fractures cutting thick silicified fault breccia soling into the basal shear zone, suggesting some slip localization following silicification at this mechanical contrast (f).

responses to those of a minimally altered granodiorite. The strength contrast between fault core and the adjacent wall rock, as well as structural and mineralogical descriptions of the fault core in each area, are summarized in Table 3.

5. Discussion

5.1. Mechanisms of fault core widening at Dixie Comstock

Based on characteristic breccia textures and footwall features we observe in outcrop and thin section, we infer two mechanisms of fault core widening: 1) cycles of cementation, embrittlement, deformation, and dilation of the fault core, and 2) stepping of the fault core into the footwall by plucking and entrainment of adjacent damage zone material. Silicification resulted in increased strength, stiffness, and brittleness (Table 2), thus promoting dilatancy upon failure. Evidence for dilation includes re-brecciation of previously cemented breccia components, cockade breccia, and multiple generations of mutually crosscutting veins cutting previously cemented clasts (Figs. 5, 10c and 11). Repeated stages of dilation and cementation indicate that locally the fault core widened concomitant with mineralization. Widening of the fault core by widespread plucking and cementation of footwall material and apparent roughening of the basal fault rather than through incremental wear, grain size reduction, and smoothing is indicated by incorporation of centimeter- to meter-scale blocks of altered footwall into the silicified breccia (Figs. 5 and 10a, b, c). Various geometries of cemented footwall fractures and damage zone blocks are observed at Dixie Comstock, including ripout clasts (Fig. 10b and c) and lozenges bound by footwall fractures (Fig. 12a). Similar features may form in the hanging wall, but direct evidence is lacking at Dixie Comstock, where the hanging wall is either poorly preserved or missing from surface exposures of the main fault and is composed of finer grained tuff and locally derived alluvium that is difficult to distinguish in the silicified fault core. Footwall ripout clasts share geometry with ripout features described in strike slip faults

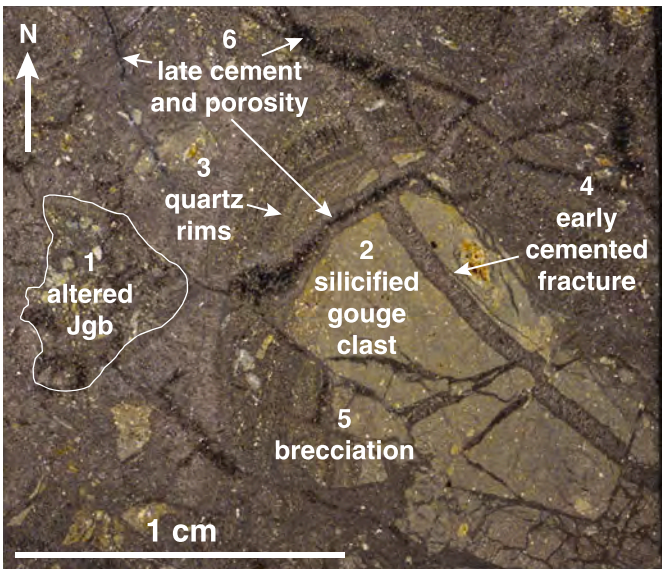

Fig. 11. Thin section showing multiple episodes of deformation, dilation, and cementation recorded in silicified fault breccia from the southern part of Area 3 (Fig. 9).

(Swanson, 1989, 2005), with fragmented wall rock in other mineralizing systems (Micklethwaite, 2009), and with millimeter-scale injection features in the footwall at the Dixie Valley Mirrors normal fault exposure (Candela and Renard, 2012). However, in the epithermal environment, ripout clasts appear displaced into the silicified fault core through dilation and cementation of the basal fracture, rather than through sliding alone (cf. Swanson, 1989, 2005). Cementation of wide, deeply penetrating, sub-vertical, fault-perpendicular cross-fractures like those described at fault step-overs by Kattenhorn et al. (2000) and asymptotic, curving-upward, dilatant pinnate fractures bound by subparallel slip surface described in other fault systems by Bruhn et al. (1994) and Micklethwaite (2009) help to isolate and encapsulated lozenges of variably weakened footwall material (Fig. 12a and b). Cementation of or around fault asperities may have contributed to instability of the principal slip surface (Fig. 12c).

5.2. *Strengthened or weakened fault cores as endmembers in diverse hydrothermal regimes*

Fluid-assisted chemical alteration resulting in the generation of phyllosilicates is commonly attributed with fault rock weakening and strain localization (Chester and Logan, 1986; Chester et al., 1993; Bruhn et al., 1994; Chester and Chester, 1998; Jefferies et al., 2006; Lockner et al., 2009; Solum et al., 2010; Sutherland et al., 2012; Barth et al., 2013; Toy et al., 2015) and may contribute to aseismic slip (Blenkinsop and Sibson, 1992; Lockner et al., 2011; Barth et al., 2013; Moore and Lockner, 2013; Bradbury et al., 2014). Fault-rock weakening is thought to contribute to strain localization onto discrete slip surfaces or intervals through focused deformation, alteration, and increase ductility. Fault-core widening in these environments is thought to occur through the gradual wear and incorporation of fault zone asperities as faults accumulate slip (Chester and Chester, 1998; Wilson et al., 2003; Sagy and Brodsky, 2009; Brodsky et al., 2011). Conversely, the wide fault core, mineralized breccia, and distributed veins and stockwork we describe at Dixie Comstock are commonly observed in other fault-hosted epithermal and porphyry deposits (Simmons et al., 2005; Micklethwaite, 2009; Jensen et al., 2019). In these environments, mineralization and cementation with common gangue minerals such as quartz or calcite, may help roughen, widen, or strengthen faults (Woodcock et al., 2007; Nortje et al., 2011). In this regard, fluid-rock interactions that either weaken or strengthen fault rocks may be considered end member hydrothermal environments that help govern the mechanical and structural evolution of fault zones.

Precipitation-strengthening and alteration-weakening may occur at the same time in different parts of the same fault system, or at different times in the same part of the fault system (Solum et al., 2010). For instance, in southern Dixie Valley conditions that favored the generation of phyllosilicates promoted alteration-weakening of the fault core (Bruhn et al., 1994; Callahan et al., 2019), whereas

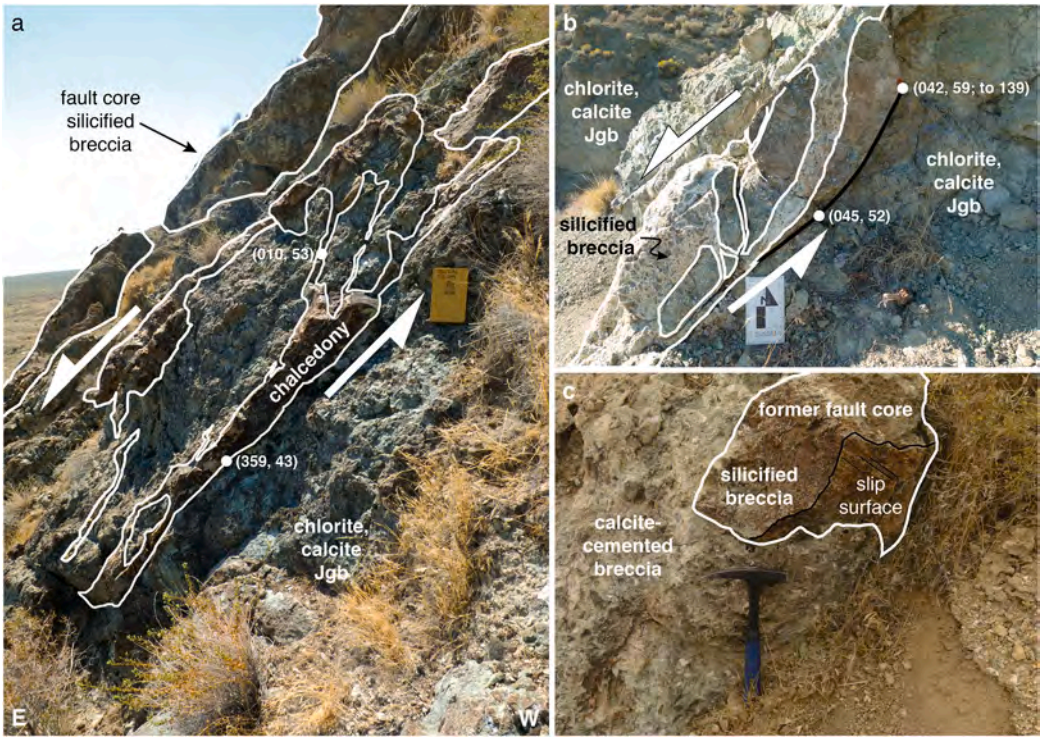

Fig. 12. Footwall detail from northern silicified facet, Area 3. Curved, mixed-mode and dilatant pinnate fractures with chalcedony and quartz-cemented graded breccia forming between slip surfaces in sheared, calcite-chlorite +quartz altered gabbro (a, b). Altered footwall material between these fractures may become incorporated into the silicified fault core if deformation and cementation extend deeper into the fault damage zone. Large block of silicified fault breccia with relict slip surface in massive, calcite-supported breccia (c). Incorporation of this block suggests instability of principal slip surface through time. Calcite breccia is also incorporated into some silicified breccias, consistent with repeated cycles of deformation and cementation under varying chemical conditions.

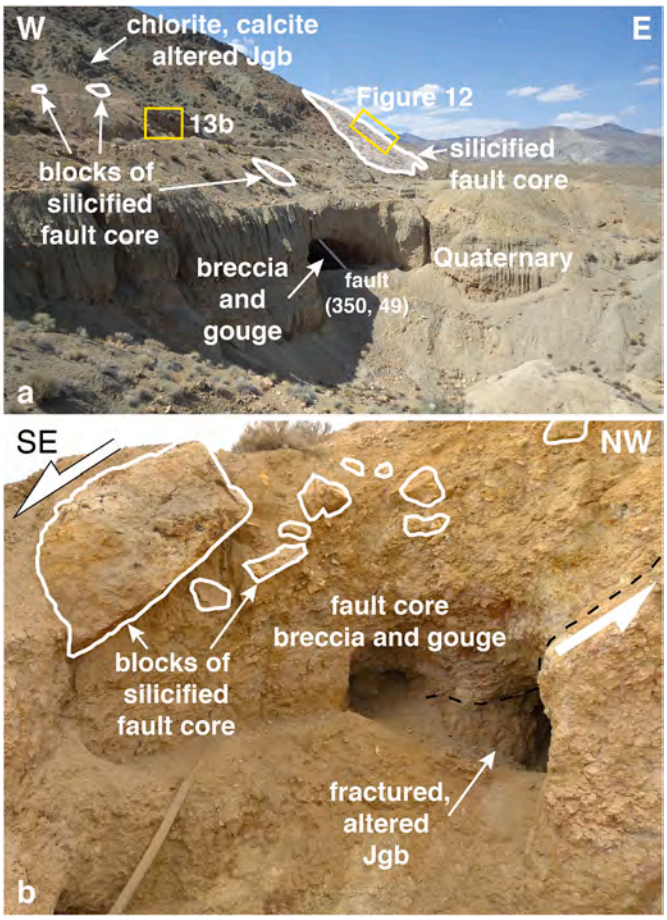

Fig. 13. Range front fault exposed in the immediate vicinity of the mine, Area 4. The topographic range front steps into chlorite, calcite, and clay-rich gabbro in the footwall, behind a former silicified facet (a). Relict, mature fault core exposed in mine workings as meter-scale blocks of silicified fault breccia contained in clay-rich fault gouge and breccia (b). Modern primary slip surface is exposed in the mine workings (a) east of inset (b).

precipitation-dominated hydrothermal regimes at the Mirrors (Caine et al., 2010; Callahan et al., 2019) and at Dixie Comstock (Callahan et al. (2019); this study) promoted and preserved strong, thick fault cores. Because hydrothermal flow can be focused and ephemeral, the impacts of fluid-rock interaction and precipitation-strengthening or alteration-weakening impart additional spatial and temporal heterogeneity to fault rock properties and fault zone evolution (e.g. Davatzes and Hickman (2010); Williams et al. (2017)). A record of diverse chemical environments and water-rock interactions may be reflected in fault zone architecture, even if hydrothermal fluid flow does not persist, as we see exemplified in the relict fault breccias in Area 4 (Fig. 13).

5.3. A model of fault zone evolution in different alteration regimes

Based on our field observations of fault zone features at Dixie Comstock, we expand upon prior published conceptual models of fault initiation (Crider and Peacock, 2004; Myers and Aydin, 2004; Crider, 2015) and models of fault architectural evolution governed by antecedent structures or frictional-wear described above to explicitly consider the variable influence and degree of localized water-rock interactions, be they weakening or strengthening, on mechanical and fault architectural elements resolved into the following five stages (Fig. 14):

1. ***Inheritance*** influences the early development of faults (Crider and Peacock, 2004; Crider, 2015), and may include the distribution of discontinuities (faults, opening mode and sheared fractures, veins, or other fabrics) and mechanical contrast arising from variations in lithology or prior alteration.
2. ***Reactivation*** involves the shear reactivation and linkage of optimally oriented inherited structures and the formation and growth of new fractures with increasing deformation (Moir et al., 2010), similar to the early and intermediate shear stage of Myers and Aydin (2004).
3. ***Fault formation*** ultimately results from coalescence and the development of through-going, discrete slip surfaces, which may include intervals of mechanical fault breccia, cataclasite, or gouge bounded by inherited and early fault structures (Fig. 6).

4a. ***Alteration-weakening and slip localization*** may occur when or where fault-enhanced, fluid-rock interactions producing fault cores rich in phyllosilicates or other weak minerals facilitate fault localization and potentially reducing overall fault strength (Fig. 14, inset). Alteration products may form in any stage of fault development but is enhanced by grain-size reduction and higher water-rock ratios as faults accumulate slip.

4b. ***Precipitation-strengthening and fault core widening*** may occur when or where fault-enhanced, fluid-rock interactions result in mineral precipitation and fault rock strengthening. The tendency for faults to experience alteration-weakening or precipitation-strengthening is controlled by the specific mineral reactions occurring within a given rock in a given hydrothermal regime, and may be influenced by predictable and mappable trends in water-rock ratios, temperature (depth), and fluid or rock chemistry (Fig. 14, inset). Repeated cycles of deformation and cementation in the precipitation-strengthening regime promote fault core widening through mineralization-embrittlement, dilation, and healing (Fig. 11), migration of slip into the damage zone below the cemented core (e. g. basal faults in Figs. 7 and 10)

Table 2
Rock and fracture mechanical properties in different fault settings (Callahan et al., 2019, 2020).

Fault Setting	Area	Alteration Minerals	Sample[a]	UCS[b] (MPa)		E[c] (GPa)		ν[d]		G[e] (GPa)		n	K_{IC}[f] (MPa $\sqrt{m}$)		
				mean	±std	mean	±std	mean	±std	mean	±std		mean	±std	n
footwall gabbro	2	minor chl, alb	083114-2A	–	–	–	–	–	–	–	–	–	0.68	0.20	14
damage zone	3, 4	chl, min cal, alb	052815-3B	50.7	–	22.8	–	0.20	–	9.5	–	1	0.56	0.13	8
damage zone	3, 4	chl, cal, alb	052815-3A	148.0	–	48.2	–	0.22	–	19.7	–	1	2.12	0.23	7
silicified fault core	3	silicified	090114-5B	301.3	38.4	58.1	0.8	0.18	0.01	24.7	0.4	3	2.40	0.16	16
silicified fault core	3	silicified	061114-4B	187.8	–	51.1	–	0.13	–	22.6	–	1	2.67	0.44	10
silicified fault core	3	silicified	052815–2	286.5	12.7	62.8	1.6	0.11	0.02	28.3	0.3	2	3.20	0.33	10

[a] Sample locations are shown on supplemental Map S1.
[b] Unconfined compressive strength.
[c] Young's modulus.
[d] Poisson's ratio.
[e] Shear modulus.
[f] Fracture toughness.

Table 3
Summary of structural, mineralogical, and mechanical properties of fault core, dixie comstock, NV.

Area	Nature of Fault Core	Features in Fault Core	Alteration and Mineralization[a]	Relative Fault Rock Strength†
1	Uncemented	~10 cm of fault breccia and foliated gouge.	phyllosilicates in gouge	fault core ≪ damage zone
2	Weakly Cemented	1–2 m thick coarse, partially quartz-cemented chaotic breccia of gabbro clasts ± multiple anastomosing slip surfaces on thin intervals of less cohesive gouge and breccia and well-developed slicken surfaces at the top.	minor quartz cement in fault breccia of ±chloritized gabbro clasts and late calcite veneer	fault core ≅ damage zone
3	Silicified	>5 m thick sheets and pods of silicified fault breccias, quartz veins, and blocks of altered gabbro clasts. Slicken lines on exposed top surface and abrupt basal fault with foliated cataclasite ±ripouts. Cut by long, steep, fault-perpendicular fractures filled or lined with quartz ±calcite that commonly extend into the footwall, and open, fault-parallel fractures that truncate at or curve into a basal fault.	Massive silicification. Quartz and ±calcite cement in cockade and graded breccia with chalcedony and chlorite, calcite, albite, ±epidote, ±sericite altered gabbro clasts. Quartz, ±sulfide and late calcite veins and areas of late, calcite supported breccia.	fault core ≫ damage zone
4	Disaggregated	>10 m thick interval of fault gouge and breccia with large (>1 m) blocks of silicified fault breccia and multiple internal slip surfaces	Montmorillonite, sericite, kaolinite, feldspar, quartz and relict blocks of silicified core	fault core ≤ damage zone

[a] From field observations, Callahan et al. (2019), and Vikre (1993). †From field observations and Table 2.

(Goodwin and Tikoff, 2002), and the incorporation of damage zone material through plucking, entrainment, and cementation (Figs. 5, 10b and 12a, b). Dilation and enhanced permeability may occur within the mineralized and embrittled fault core during coseismic failure when deformation outpaces precipitation.

5. ***Fault core disaggregation*** may occur as continued deformation distributes blocks of the remnant fault core through a wide matrix of fault rock and gouge (Fig. 13). Slip may localize in the weakened material but evidence for prior precipitation-strengthening and wide fault cores may be preserved as entrained clasts of cemented fault breccia.

5.4. Implications of precipitation-strengthening on models of fault evolution and behavior

In the most cemented state, precipitation-strengthened fault cores may be stronger and less hydraulically conductive than incipient faults, early faults, and mature, alteration-weakened fault systems. However, we also demonstrated that mineralization may embrittle the fault core, thus promoting slip dilatancy and facilitating transient upwelling of hydrothermal fluids following coseismic deformation. In this way, precipitation-strengthening may provide an additional positive feedback mechanism where previously cemented, embrittled, and dilatant fault segments remain local, episodic conduits along structurally active faults (e.g. Sibson (1987); Grare et al. (2018)). In the model we propose, fault cores experiencing precipitation-strengthening also become wider than faults influenced by alteration-weakening and slip localization. Thus, complex fault zone architecture is not only a control on fluid flow (e.g. Caine et al. (1996)), but may also be a *consequence* of fluid flow and fluid-rock interactions (e.g. Sosio De Rosa et al. (2018); Menezes et al. (2019)).

Mineral precipitation, cementation, and fault core strengthening likely contributed to the development and preservation of fault zone elements in some exceptional exposures described in impactful field investigations of faults and fluids (Power and Tullis, 1989, 1992; Eichhubl and Boles, 2000a; Eichhubl and Boles, 2000b; Boles et al., 2004; Benedicto et al., 2008; Sagy and Brodsky, 2009; Caine et al., 2010; Candela and Renard, 2012; Kirkpatrick et al., 2013; Collettini et al., 2014; Ferraro et al., 2019). Outcrops in these studies are exceptional in part because fault textures and changes in the composition of fault-hosted fluids are preserved in cements, providing a more robust record of deformation and paleo-flow conditions than fault systems dominated by comminution alone. However, if faults in the precipitation-strengthening regime demonstrate different mechanical and hydrological behavior than faults in the alteration-weakening regime (Fig. 14, inset), it follows that inferences about fault zone properties and processes based on well-cemented faults may not apply to weak, clay-rich portions of fault systems, and *vice versa*. Therefore, we suggest that identifying the physiochemical environment and specific alteration products in models of subsurface fault zone architecture and behavior may help reduce bias and improve assessment of fault-controlled mineral and hydrothermal resources, oil, gas, and CO_2 sequestration reservoirs, and seismic hazard associated with active faults (Scibek et al., 2016; Shipton et al., 2019).

6. Conclusions

Economic gold concentrations at the Dixie Comstock epithermal deposit are a result of localized advection of mineralizing fluids. Within and adjacent to this deposit, we observed variation in fault core width, cementation, and deformation mechanisms. Minor background faults in regionally metasomatized gabbro contain thin cores of foliated fault gouge. With increasing silicification we observe increased fault core width, resulting from embrittlement, brecciation, dilation, and cementation, as well as the incorporation and encapsulation of footwall damage zone material. Post-silicification deformation of the fault core ultimately resulted in disaggregation of previously cemented breccia into a wide matrix of fault gouge. Mechanical testing of altered footwall and fault core breccia reveal significant increases in strength as a result of silicification. Based on these observations, we present a broader conceptual model of fault zone evolution that includes paths through alteration-weakening or precipitation-strengthening regimes, with observable differences in mature fault zone architecture. Implicit in this model is that interactions between deformation, alteration, mineralization, and fluid flow in different hydrothermal regimes not only arise from but contributed to the development of along strike variations in fault zone architecture and hydromechanical behavior. In the epithermal environment, interactions between focused advection, boiling, and cooling of silica-rich fluids results in mineral precipitation, strengthening, and widening of the fault core. Mineralization-embrittlement and resulting dilatancy may have enhanced transient, coseismic permeability within the fault core and helped to further localize shallow mineralization. Conceptual models of fault zone

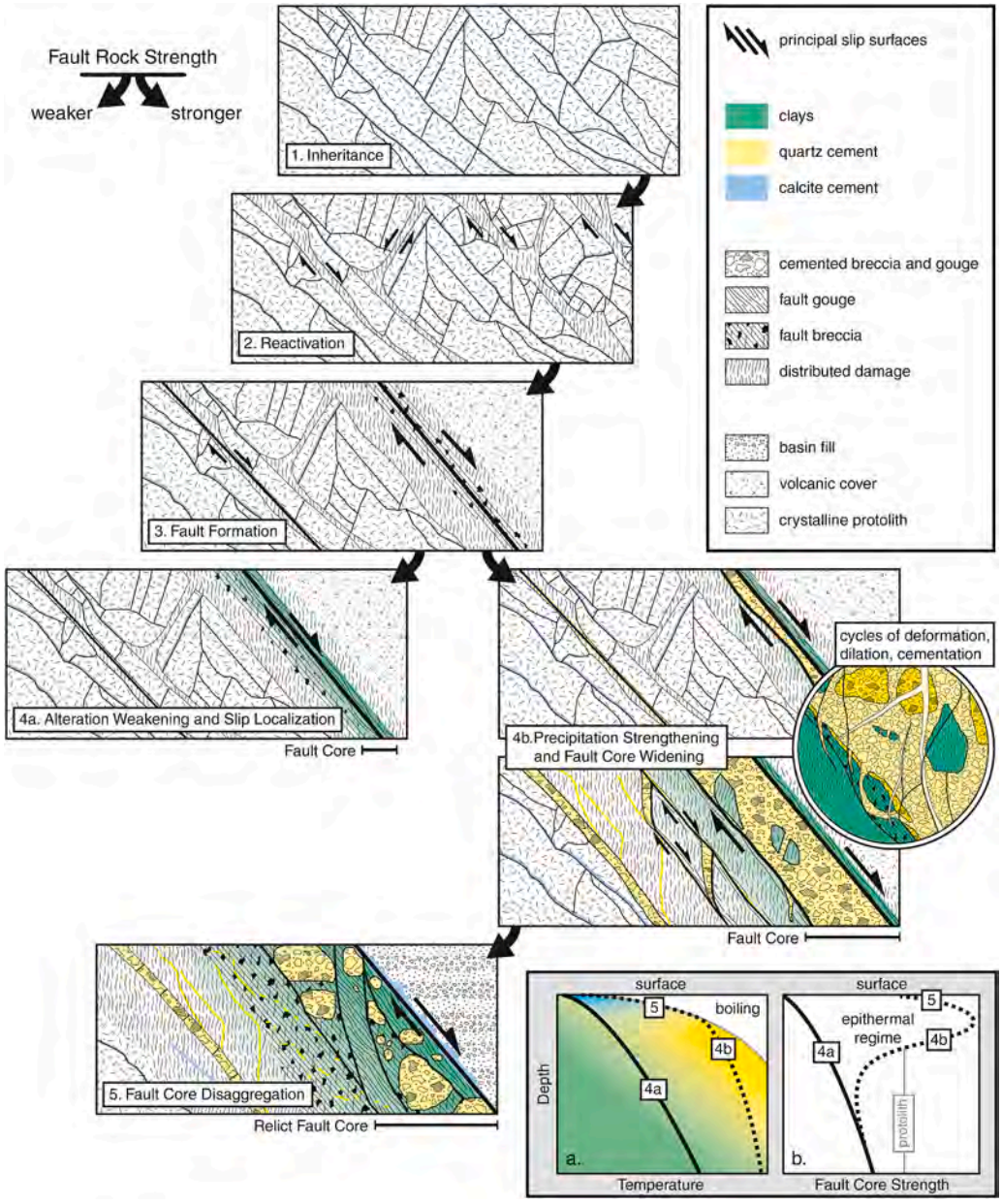

Fig. 14. Conceptual model of fault zone evolution in alteration-weakening and precipitation-strengthening regimes based on field observations of the footwall at Dixie Comstock epithermal deposit. 1 to 3) Early fault formation and localization in previously altered and damaged host rock. 4a) Enhanced fluid-rock interaction in the fault zone resulting in alteration-weakening. 4b) Precipitation-strengthening in mineralizing, precipitation-dominated environment, resulting in fault core widening and fault rock strengthening through repeated cycles of deformation, fault core dilation, and cementation as well as incorporation of adjacent footwall blocks. 5) Disaggregation of the silicified fault core as deformation outpaces cementation. Deformation within the hanging wall is not constrained in outcrop. Tendency toward weakening or strengthening of the fault core and associated differences in fault zone architecture reflect differences in the hydrothermal regime during deformation (inset): a) Hypothetical temperature-depth distributions and dominant alteration (color shading) under typical geothermal gradients (solid line) and in epithermal environments (dashed line) in the shallow crust. Occurrence of fault evolutionary stages 4a vs 4b, and 5, shown. b) Extrapolated depth-fault core strength distributions based on (a) (modified from Callahan et al., 2019). (For interpretation of the references to color in this figure legend, the reader is referred to the Web version of this article.)

evolution that include divergent paths based on subsurface chemical conditions and reactions may help improve predictions of the hydro-mechanical and seismogenic behavior of faults.

CRediT authorship contribution statement

Owen A. Callahan: Conceptualization, Investigation, Writing - original draft, Writing - review & editing, Visualization, Funding acquisition, Data curation. **Peter Eichhubl:** Conceptualization, Investigation, Resources, Writing - review & editing, Funding acquisition, Supervision. **Nicholas C. Davatzes:** Conceptualization, Investigation, Writing - review & editing.

Declaration of competing interest

The authors declare that they have no known competing financial interests or personal relationships that could have appeared to influence the work reported in this paper.

Acknowledgements

Support for this research was provided by the GDL Foundation, the Geothermal Resources Council, and the AAPG Foundation. Additional support was provided by The Jackson School of Geosciences at The University of Texas at Austin, the Fracture Research and Application Consortium (FRAC), and a Publication Grant from the Bureau of Economic Geology. Sol Cooperdock, Adenike Tokan-Lawal, and Alison MacNamee assisted with fieldwork. Robin Zuza, Ormat Technologies, Inc., shared lithologic information from geothermal exploration wells. Billy J. Andrews and Randy Williams provided prompt and thoughtful reviews. Publication authorized by the Director, Bureau of Economic Geology.

Data Availability

Supplemental data related to this article can be found at https://doi.org/10.17632/tfvfk86c8s.2 an open-source online data repository hosted at Mendeley Data (Callahan et al., 2020).

References

Backeberg, N.R., Rowe, C.D., Barshi, N., 2016. Alteration-weakening leading to localized deformation in a damage aureole adjacent to a dormant shear zone. J. Struct. Geol. 90, 144–156. https://doi.org/10.1016/j.jsg.2016.07.008.

Barth, N.C., Boulton, C., Carpenter, B.M., Batt, G.E., Toy, V.G., 2013. Slip localization on the southern alpine fault, New Zealand. Tectonics 32, 620–640. https://doi.org/10.1002/tect.20041.

Becker, G.F., Ransome, F.L., 1928. Geologic Map of the Mother Lode Belt. California.

Bell, J.W., Caskey, S.J., Ramelli, A.R., Guerrieri, L., 2004. Pattern and rates of faulting in the Central Nevada Seismic Belt, and paleoseismic evidence for prior beltlike behavior. Bull. Seismol. Soc. Am. 94 (4), 1229–1254. https://doi.org/10.1785/012003226.

Benedicto, A., Plagnes, V., Vergély, P., Flotté, N., Schultz, R.A., 2008. Fault and fluid interaction in a rifted margin: integrated study of calcite-sealed fault-related structures (southern Corinth margin). Geological Society, London, Special Publications 299 (1), 257–275. https://doi.org/10.1144/sp299.16.

Benoit, D., 1992. A case history of injection through 1991 at Dixie Valley, Nevada. Geothremal Resources Council Transactions 16, 611–620.

Bense, V.F., Gleeson, T., Loveless, S.E., Bour, O., Scibek, J., 2013. Fault zone hydrogeology. Earth Sci. Rev. 127, 171–192. https://doi.org/10.1016/j.earscirev.2013.09.008.

Blackwell, D.D., Golan, B., Benoit, D., 2000. Temperatures in the Dixie Valley, Nevada geothermal system. GRC Transactions 24, 223–228.

Blackwell, D.D., Smith, R.P., Richards, M.C., 2007. Exploration and Development at Dixie Valley, Nevada: Summary of DOE Studies. Paper Presented at the 32nd Workshop on Geothermal Reservoir Engineering. Stanford University, Stanford, California.

Blanpied, M.L., Lockner, D.A., Byerlee, J.D., 1995. Frictional slip of granite at hydrothermal conditions. J. Geophys. Res. 100 (B7) https://doi.org/10.1029/95jb00862, 13045.

Blanpied, M.L., Marone, C.J., Lockner, D.A., Byerlee, J.D., King, D.P., 1998. Quantitative measure of the variation in fault rheology due to fluid-rock interactions. J. Geophys. Res. 103 (B5) https://doi.org/10.1029/98jb00162, 9691.

Blenkinsop, T.G., Sibson, R.H., 1992. Aseismic fracturing and cataclasis involving reaction softening within core material from the Cajon Pass drill hole. Journal of Geophysical Research - Solid Earth 97 (B4), 5135–5144. https://doi.org/10.1029/90JB02285.

Boles, J.R., Eichhubl, P., Garven, G., Chen, J., 2004. Evolution of a hydrocarbon migration pathway along basin-bounding faults: evidence from fault cement. AAPG (Am. Assoc. Pet. Geol.) Bull. 88 (7), 947–970. https://doi.org/10.1306/02090403040.

Bradbury, K.K., Davis, C.R., Shervais, J.W., Janecke, S.U., Evans, J.P., 2014. Composition, alteration, and texture of fault-related rocks from SAFOD core and surface outcrop analogs: evidence for deformation processes and fluid-rock interactions. Pure Appl. Geophys. 172 (5), 1053–1078. https://doi.org/10.1007/s00024-014-0896-6.

Brodsky, E.E., Gilchrist, J.J., Sagy, A., Collettini, C., 2011. Faults smooth gradually as a function of slip. Earth Planet Sci. Lett. 302 (1–2), 185–193. https://doi.org/10.1016/j.epsl.2010.12.010.

Bruhn, R.L., Parry, W.T., Yonkee, W.A., Thompson, T., 1994. Fracturing and hydrothermal alteration in normal fault zones. Pure Appl. Geophys. 142 (3/4), 609–644. https://doi.org/10.1007/BF00876057.

Caine, J.S., 1999. The Architecture and Permeability Structure of Brittle Fault Zones. (PhD). University of Utah.

Caine, J.S., Bruhn, R.L., Forster, C.B., 2010. Internal structure, fault rocks, and inferences regarding deformation, fluid flow, and mineralization in the seismogenic Stillwater normal fault, Dixie Valley, Nevada. J. Struct. Geol. vol. 32 (11), 1576–1589. https://doi.org/10.1016/j.jsg.2010.03.004.

Caine, J.S., Evans, J.P., Forster, C.B., 1996. Fault zone architecture and permeability structure. Geology *24* (11), 1025–1028. https://doi.org/10.1130/0091-7613(1996)024<1025:fzaaps>2.3.co;2.

Callahan, O.A., Eichhubl, P., Olson, J.E., Davatzes, N.C., 2019. Fracture mechanical properties of damaged and hydrothermally altered rocks, Dixie Valley-Stillwater fault zone, Nevada, USA. J. Geophys. Res.: Solid Earth 124 (4), 4069–4090. https://doi.org/10.1029/2018jb016708.

Callahan, O.A., Eichhubl, P., Olson, J.E., Davatzes, N.C., 2020. Experimental investigation of chemically aided fracture growth in silicified fault rocks. Geothermics 83. https://doi.org/10.1016/j.geothermics.2019.101724.

Candela, T., Renard, F., 2012. Segment linkage process at the origin of slip surface roughness: evidence from the Dixie Valley fault. J. Struct. Geol. 45, 87–100. https://doi.org/10.1016/j.jsg.2012.06.003.

Candela, T., Renard, F., Bouchon, M., Schmittbuhl, J., Brodsky, E.E., 2011. Stress drop during earthquakes: effect of fault roughness scaling. Bull. Seismol. Soc. Am. 101 (5), 2369–2387. https://doi.org/10.1785/0120100298.

Carena, S., Friedrich, A.M., 2018. Vertical-displacement history of an active Basin and Range fault based on integration of geomorphologic, stratigraphic, and structural data. Geosphere 14 (4), 1657–1676. https://doi.org/10.1130/ges01600.1.

Caskey, S.J., Ramelli, A.R., 2004. Tectonic displacement and far-field isostatic flexure of pluvial lake shorelines, Dixie Valley, Nevada. J. Geodyn. 38 (2), 131–145. https://doi.org/10.1016/j.jog.2004.06.001.

Caskey, S.J., Wesnousky, S.G., Zhang, P., Slemmons, D.B., 1996. Surface faulting of the 1954 Fairview Peak (M_s 7.2) and Dixie Valley (M_s 6.8) earthquakes, central Nevada. Bull. Seismol. Soc. Am. 86 (3), 761–787.

Chen, J., Verberne, B.A., Spiers, C.J., 2015. Interseismic re-strengthening and stabilization of carbonate faults by "non-Dieterich" healing under hydrothermal conditions. Earth Planet Sci. Lett. 423, 1–12. https://doi.org/10.1016/j.epsl.2015.03.044.

Chester, F.M., Chester, J.S., 1998. Ultracataclasite structure and friction processes of the Punchbowl fault, San Andreas system, California. Tectonophysics 295, 199–221. https://doi.org/10.1016/S0040-1951(98)00121-8.

Chester, F.M., Evans, J.P., Biegel, R.L., 1993. Internal structure and weakening mechanisms of the San Andreas Fault. J. Geophys. Res. 98, 771–786. https://doi.org/10.1029/92JB01866.

Chester, F.M., Logan, J.M., 1986. Implications for mechanical properties of brittle faults from observations of the Punchbowl fault zone, California. PAGE 124 (1/2), 79–106. https://doi.org/10.1007/BF00875720.

Childs, C., Manzocchi, T., Walsh, J.J., Bonson, C.G., Nicol, A., Schöpfer, M.P.J., 2009. A geometric model of fault zone and fault rock thickness variations. J. Struct. Geol. 31 (2), 117–127. https://doi.org/10.1016/j.jsg.2008.08.009.

Childs, C., Watterson, J., Walsh, J.J., 1996. A model for the structure and development of fault zones. J. Geol. Soc. 153, 337–340.

Choi, J.-H., Edwards, P., Ko, K., Kim, Y.-S., 2016. Definition and classification of fault damage zones: a review and a new methodological approach. Earth Sci. Rev. 152, 70–87. https://doi.org/10.1016/j.earscirev.2015.11.006.

Collettini, C., Carpenter, B.M., Viti, C., Cruciani, F., Mollo, S., Tesei, T., et al., 2014. Fault structure and slip localization in carbonate-bearing normal faults: an example from the Northern Apennines of Italy. J. Struct. Geol. 67, 154–166. https://doi.org/10.1016/j.jsg.2014.07.017.

Collettini, C., Niemeijer, A., Viti, C., Marone, C., 2009. Fault zone fabric and fault weakness. Nature 462 (7275), 907–910. https://doi.org/10.1038/nature08585.

Cowie, P.A., 1998. A healing-reloading feedback control on the growth rate of seismogenic faults. J. Struct. Geol. 20 (8), 1075–1087. https://doi.org/10.1016/S0191-8141(98)00034-0.

Cox, S.F., 2005. Coupling between deformation, fluid pressure, and fluid flow in ore-producing hydrothermal systems at depth in the crust. In: Economic Geology 100th Anniversary. Society of Economic Geology, pp. 39–75.

Crider, J.G., 2015. The initiation of brittle faults in crystalline rock. J. Struct. Geol. 77, 159–174. https://doi.org/10.1016/j.jsg.2015.05.001.

Crider, J.G., Peacock, D.C.P., 2004. Initiation of brittle faults in the upper crust: a review of field observations. J. Struct. Geol. 26, 691–707. https://doi.org/10.1016/j.jsg.2003.07.007.

Davatzes, N.C., Aydin, A., Eichhubl, P., 2003. Overprinting faulting mechanisms during the development of multiple fault sets in sandstone, Chimney Rock fault array, Utah, USA. Tectonophysics 363 (1–2), 1–18. https://doi.org/10.1016/s0040-1951(02)00647-9.

Davatzes, N.C., Hickman, S.H., 2010. The feedback between stress, faulting, and fluid flow: lessons from the Coso Geothermal Field, CA, USA. In: Proceedings, World Geothermal Congress.

Dewhurst, D.N., Jones, R.M., 2003. Influence of physical and diagenetic processes on fault geomechanics and reactivation. J. Geochem. Explor. 78–79, 153–157. https://doi.org/10.1016/s0375-6742(03)00124-9.

Dilek, Y., Moores, E.M., 1995. Geology of the Humboldt igneous complex, Nevada, and tectonic implications for the Jurassic magmatism in the Cordilleran orogen. In: Miller, D.M., Busby, C. (Eds.), Jurassic Magmatism and Tectonics of the North American Cordillera. Geological Society of America Special, Boulder, Colorado, pp. 229–248. https://doi.org/10.1130/SPE299-p229. Paper 299.

Eichhubl, P., Boles, J.R., 2000a. Focussed fluid flow along faults in the Monterey Formation, coastal California. GSA Bulletin 112 (11), 1667–1679. https://doi.org/10.1130/0016-7606(2000)112<1667:FFFAFI>2.0.CO;2.

Eichhubl, P., Boles, J.R., 2000b. Rates of fluid flow in fault systems; evidence for episodic rapid fluid flow in the Miocene Monterey Formation, coastal California. Am. J. Sci. 300 (7), 571–600. https://doi.org/10.2475/ajs.300.7.571.

Eichhubl, P., Davatzes, N.C., Becker, S.P., 2009. Structural and diagenetic control of fluid migration and cementation along the Moab fault, Utah. AAPG (Am. Assoc. Pet. Geol.) Bull. 93 (5), 653–681. https://doi.org/10.1306/02180908080.

Escartin, J., Hirth, G., Evans, B., 2001. Strength of slightly serpentinized peridotites: implications for the tectonics of oceanic lithosphere. Geology *29* (11), 1023–1026. https://doi.org/10.1130/0091-7613(2001)029<1023:SOSSPI>2.0.CO;2.

Evans, J.P., Forster, C.B., Goddard, J.V., 1997. Permeability of fault-related rocks, and implications for hydraulic structure of fault zones. J. Struct. Geol. 19 (11), 1393–1404.

Faulkner, D.R., Jackson, C.A.L., Lunn, R.J., Schlische, R.W., Shipton, Z.K., Wibberley, C.A.J., Withjack, M.O., 2010. A review of recent developments concerning the structure, mechanics and fluid flow properties of fault zones. J. Struct. Geol. 32 (11), 1557–1575. https://doi.org/10.1016/j.jsg.2010.06.009.

Faulkner, D.R., Mitchell, T.M., Rutter, E.H., Cembrano, J., 2008. On the structure and mechanical properties of large strike-slip faults. In: Wibberley, C.A.J., Kurz, W., Imber, J., Holdsworth, R.E., Collettini, C. (Eds.), The Internal Structure of Fault Zones: Implications for Mechanical and Fluid-Flow Properties, vol. 299. Geological Society, London, pp. 139–150. https://doi.org/10.1144/SP299.9.

Ferraro, F., Agosta, F., Ukar, E., Grieco, D.S., Cavalcante, F., Belviso, C., Prosser, G., 2019. Structural diagenesis of carbonate fault rocks exhumed from shallow crustal

depths: an example from the central-southern Apennines, Italy. J. Struct. Geol. 122, 58–80. https://doi.org/10.1016/j.jsg.2019.02.008.
Gonsior, Z.J., Dilles, J.H., 2008. Timing and evolution of Cenozoic extensional normal faulting and magmatism in the southern Tobin Range, Nevada. Geosphere 4 (4), 687–712. https://doi.org/10.1130/GES00137.1.
Goodwin, L.B., Tikoff, B., 2002. Competency contrast, kinematics, and the development of foliations and lineations in the crust. J. Struct. Geol. 24 (6–7), 1065–1085. https://doi.org/10.1016/S0191-8141(01)00092-X.
Grare, A., Lacombe, O., Mercadier, J., Benedicto, A., Guilcher, M., Trave, A., et al., 2018. fault zone evolution and development of a structural and hydrological barrier: the quartz breccia in the Kiggavik area (Nunavut, Canada) and its control on uranium mineralization. Minerals 8 (8). https://doi.org/10.3390/min8080319.
Gratier, J.P., 2011. Fault permeability and strength evolution related to fracturing and healing episodic processes (years to millenia): the role of pressure solution. Oil Gas Sci. Technol. 1–16. https://doi.org/10.2516/ogst/2010014.
Hickman, S., Zoback, M., Benoit, R., 1998. Tectonic Controls on Reservoir Permeability in the Dixie Valley, Nevada, Geothermal Field. Paper Presented at the 23rd Workshop on Geothermal Reservoir Engineering. Stanford University, Stanford, CA.
Hickman, S.H., Barton, C.A., Zoback, M.D., Morin, R., Sass, J., Benoit, R., 2007. In-situ stress and fracture permeability along the Stillwater fault zone, Dixie Valley, Nevada. Int. J. Rock Mech. Min. Sci. 34 (3–4) https://doi.org/10.1016/S0148-9062(97)00169-1.
Hickman, S.H., Zoback, M.D., Barton, C.A., Benoit, R., Svitek, J., Summers, R., 2000. Stress and permeability heterogeneity within the Dixie Valley geothermal reservoir: recent results from Well 82-5. Paper Presented at the 25th Workshop on Geothermal Reservoir Engineering. Stanford University, Stanford, California.
Hudson, M.R., Geissman, J.W., 1991. Paleomagnetic evidence for the age and extent of middle Tertiary counterclockwise rotation, Dixie Valley region, west central Nevada. J. Geophys. Res. 96 (B3), 3979–4006. https://doi.org/10.1029/90JB02424.
Hull, J., 1988. Thickness-displacement relationships for deformation zones. J. Struct. Geol. 10, 431–435. https://doi.org/10.1016/0191-8141(88)90020-X.
Ikari, M.J., Niemeijer, A.R., Marone, C., 2011. The role of fault zone fabric and lithification state on frictional strength, constitutive behavior, and deformation microstructure. J. Geophys. Res. 116 (B8) https://doi.org/10.1029/2011jb008264.
Jefferies, S.P., Holdsworth, R.E., Shimamoto, T., Takagi, H., Lloyd, G.E., Spiers, C.J., 2006. Origin and mechanical significance of foliated cataclastic rocks in the cores of crustal-scale faults: examples from the Median Tectonic Line, Japan. J. Geophys. Res.: Solid Earth 111 (B12). https://doi.org/10.1029/2005jb004205.
Jensen, E., González, G., Faulkner, D.R., Cembrano, J., Mitchell, T.M., 2019. Fault-fluid interaction in porphyry copper hydrothermal systems: faulted veins in Radomiro Tomic, northern Chile. J. Struct. Geol. 126, 301–317. https://doi.org/10.1016/j.jsg.2019.06.013.
John, D.A., 1995. Tilted middle Tertiary ash-flow calderas and subjacent granitic plutons, southern Stillwater Range, Nevada: cross sections of an Oligocene igneous center. GSA Bulletin 107 (2), 180–200. https://doi.org/10.1130/0016-7606(1995)107<0180:TMTAFC>2.3.CO;2.
Johnson, D.A., Barton, M.D., 2000. Time-space development of an external brine-dominated, igneous-driven hydrothermal system: Humboldt Mafic Compex, Western Nevada, Part I. In: Dilles, J.H., Barton, M.D., Johnson, D.A., Proffett, J.M., Einaudi, M.T. (Eds.), Contrasting Styles of Intrusion-Associated Hydrothermal Systems, vol. 32. Society of Economic Geologists, pp. 127–143.
Karner, S.L., Marone, C., Evans, B., 1997. Laboratory study of fault healing and lithificaiton in simulated fault gouge under hydrothermal conditions. Tectonophysics 277, 41–55. https://doi.org/10.1016/S0040-1951(97)00077-2.
Kattenhorn, S.A., Aydin, A., Pollard, D.D., 2000. Joints at high angles to normal fault strike: an explanation using 3-D numerical models of fault-perturbed stress fields. J. Struct. Geol. 22, 1–23. https://doi.org/10.1016/S0191-8141(99)00130-3.
Kennedy-Bowdoin, T., Silver, E.A., Martini, B.A., Pickles, W.L., 2004. Chemical and structural dynamics of a geothermal system: hyperspectral imaging and field observations, Dixie Meadows, Nevada. GRC Transactions 645–648.
Kim, Y.-S., Peacock, D.C.P., Sanderson, D.J., 2004. Fault damage zones. J. Struct. Geol. 26 (3), 503–517. https://doi.org/10.1016/j.jsg.2003.08.002.
Kirkpatrick, J.D., Rowe, C.D., White, J.C., Brodsky, E.E., 2013. Silica gel formation during fault slip: evidence from the rock record. Geology 41 (9), 1015–1018. https://doi.org/10.1130/g34483.1.
Kistler, R.W., Speed, R.C., 2000. $^{40}Ar/^{39}Ar$, K-Ar, Rb-Sr Whole Rock and Mineral Ages, Chemical Composition, Strontium, Oxygen and Hydrogen Isotopic Systematics of Jurassic Humboldt Lopolith and Permian (?) and Triassic Koipato Group Rocks, Pershing and Churchill counties, Nevada. In: Open-File Report 00-217. USGS.
Laubach, S.E., Eichhubl, P., Hargrove, P., Ellis, M.A., Hooker, J.N., 2014. Fault core and damage zone fracture attributes vary along strike owing to interaction of fracture growth, quartz accumulation, and differing sandstone composition. J. Struct. Geol. 68, 207–226. https://doi.org/10.1016/j.jsg.2014.08.007.
Lindgren, W., 1913. Mineral Deposits, 4th ed. McGraw Hill, New York.
Lockner, D.A., Morrow, C., Moore, D., Hickman, S., 2011. Low strength of deep San Andreas fault gouge from SAFOD core. Nature 472, 82–85. https://doi.org/10.1038/nature09927.
Lockner, D.A., Tanaka, H., Ito, H., Ikeda, R., Omura, K., Naka, H., 2009. Geometry of the nojima fault at nojima-hirabayashi, Japan – I. A simple damage structure inferred from borehole core permeability. Pure Appl. Geophys. 166 (10–11), 1649–1667. https://doi.org/10.1007/s00024-009-0515-0.
Lutz, S.J., Caskey, S.J., Mildenhall, D.D., Browne, P.R.L., Johnson, S.D., 2002. Dating sinter deposits in northern Dixie Valley, Nevada-the paleoseismic record and implications for the Dixie Valley geothermal system. Paper Presented at the 27th Workshop on Geothermal Reservoir Engineering. Stanford University.
Lutz, S.J., Hulen, J.B., 2000. Mapping and Characterization of Hydrothermal Alteration Associated with the Dixie Valley Geothermal System, Nevada. Department of Energy (DOE/ID-10743).
Lyakhovsky, V., Sagy, A., Boneh, Y., Reches, Z.e., 2014. Fault wear by damage evolution during steady-state slip. Pure Appl. Geophys. 171 (11), 3143–3157. https://doi.org/10.1007/s00024-014-0787-x.
MacNamee, A.F., 2015. *Thermochronometric Investigation of Structural Evolution and Geothermal Systems in Extensional Settings, Dixie Valley, Nevada.* (MS). The University of Texas at Austin.
McKay, L., Shipton, Z.K., Lunn, R.J., Andrews, B., Raub, T.D., Boyce, A.J., 2019. Detailed internal structure and along-strike variability of the core of a plate boundary fault: the Highland Boundary Fault, Scotland. J. Geol. Soc. https://doi.org/10.1144/jgs2018-226.
Menezes, C.P., Bezerra, F.H.R., Balsamo, F., Mozafari, M., Vieira, M.M., Srivastava, N.K., de Castro, D.L., 2019. Hydrothermal silicification along faults affecting carbonate-sandstone units and its impact on reservoir quality, Potiguar Basin, Brazil. Mar. Petrol. Geol. 110, 198–217. https://doi.org/10.1016/j.marpetgeo.2019.07.018.
Micklethwaite, S., 2009. Mechanisms of faulting and permeability enhancement during epithermal mineralisation: Cracow goldfield, Australia. J. Struct. Geol. 31 (3), 288–300. https://doi.org/10.1016/j.jsg.2008.11.016.
Mitchell, T.M., Faulkner, D.R., 2009. The nature and origin of off-fault damage surrounding strike-slip fault zones with a wide range of displacements: a field study from the Atacama fault system, northern Chile. J. Struct. Geol. 31 (8), 802–816. https://doi.org/10.1016/j.jsg.2009.05.002.
Moir, H., Lunn, R.J., Shipton, Z.K., Kirkpatrick, J.D., 2010. Simulating brittle fault evolution from networks of pre-existing joints within crystalline rock. J. Struct. Geol. 32 (11), 1742–1753. https://doi.org/10.1016/j.jsg.2009.08.016.
Moore, D.E., Lockner, D.A., 2013. Chemical controls on fault behavior: weakening of serpentinite sheared against quartz-bearing rocks and its significance for fault creep in the San Andreas system. J. Geophys. Res.: Solid Earth 118 (5), 2558–2570. https://doi.org/10.1002/jgrb.50140.
Moore, D.E., Lockner, D.A., Summer, R., Shengli, M., Byerlee, J.D., 1996. Strength of chrysotile-serpentinite gouge under hydrothermal conditions: can it explain a weak San Andreas fault? Geology 24 (11), 1041–1044. https://doi.org/10.1130/0091-7613(1996)024<1041:SOCSGU>2.3.CO;2.
Moore, J.C., Byrne, T., 1987. Thickening of fault zones: a mechanism of melange formation in accreting sediments. Geology 15, 1040–1043. https://doi.org/10.1130/0091-7613(1987)15<1040:TOFZAM>2.0.CO;2.
Moore, J.C., Saffer, D., 2001. Updip limit of the seismogenic zone beneath the accretionary prism of southwest Japan: an effect of diagenetic to low-grade metamorphic processes and increasing effective stress. Geology 29 (2), 183–186. https://doi.org/10.1130/0091-7613(2001)029<0183:ULOTSZ>2.0.CO;2.
Morton, N., Girty, G.H., Rockwell, T.K., 2012. Fault zone architecture of the San Jacinto fault zone in Horse Canyon, southern California: a model for focused post-seismic fluid flow and heat transfer in the shallow crust. Earth Planet Sci. Lett. 329–330, 71–83. https://doi.org/10.1016/j.epsl.2012.02.013.
Muhuri, S.K., Dewers, T.A., Scott Jr., T.E., Reches, Z.e., 2003. Interseismic fault strengthening and earthquake-slip instability: friction or cohesion? Geology 31 (10), 881–884. https://doi.org/10.1130/G19601.1.
Myers, R., Aydin, A., 2004. The evolution of faults formed by shearing across joint zones in sandstone. J. Struct. Geol. 26 (5), 947–966. https://doi.org/10.1016/j.jsg.2003.07.008.
Niwa, M., Mizuochi, Y., Tanase, A., 2015. Changes in chemical composition caused by water-rock interactions across a strike-slip fault zone: case study of the Atera Fault, Central Japan. Geofluids 15 (3), 387–409. https://doi.org/10.1111/gfl.12096.
Nortje, G.S., Oliver, N.H.S., Blenkinsop, T.G., Keys, D.L., McLellan, J.G., Oxenburgh, S., 2011. New Faults v. Fault Reactivation; Implications for Fault Cohesion, Fluid Flow and Copper Mineralization, Mount Gordon Fault Zone, Mount Isa District, Australia. In: , vol. 359. Geological Society Special Publications, pp. 287–311.
Nosker, S.A., 1981. *Stratigraphy and Structure of the Sou Hills, Pershing County, Nevada.* (PhD). University of Nevada, Reno. Retrieved from. http://hdl.handle.net/11714/1572.
Okaya, D.A., Thompson, G.A., 1985. Geometry of Cenozoic extensional faulting: Dixie Valley, Nevada. Tectonics 4 (1), 107–125. https://doi.org/10.1029/TC004i001p00107.
Olsen, M.P., Scholz, C.H., Léger, A., 1998. Healing and sealing of a simulated fault gouge under hydrothermal conditions: implications for fault healing. J. Geophys. Res. 103 (B4) https://doi.org/10.1029/97jb03402, 7421.
Ostermeijer, G.A., Mitchell, T.M., Aben, F.M., Dorsey, M.T., Browning, J., Rockwell, T.K., et al., 2020. Damage zone heterogeneity on seismogenic faults in crystalline rock; a field study of the Borrego Fault, Baja California. J. Struct. Geol. 137 https://doi.org/10.1016/j.jsg.2020.104016.
Parry, W.T., Bruhn, R.L., 1990. Fluid pressure transients on seismogenic normal faults. Tectonophysics 179, 335–344. https://doi.org/10.1016/0040-1951(90)90299-N.
Parry, W.T., Hedderly-Smith, D., Bruhn, R.L., 1991. Fluid inclusions and hydrothermal alteration on the Dixie Valley fault, Nevada. J. Geophys. Res. 96 (B12) https://doi.org/10.1029/91jb01965, 19733.
Peacock, D.C.P., Dimmen, V., Rotevatn, A., Sanderson, D.J., 2017. A broader classification of damage zones. J. Struct. Geol. 102, 179–192. https://doi.org/10.1016/j.jsg.2017.08.004.
Power, W.L., Tullis, T.E., 1989. The relationship between slickenside surface in fine-grained quartz and the seismic cycle. J. Struct. Geol. 11 (7), 879–893. https://doi.org/10.1016/0191-8141(89)90105-3.
Power, W.L., Tullis, T.E., 1992. The contact between opposing fault surfaces at Dixie Valley, Nevada, and implications for fault mechanics. J. Geophys. Res. 97 (B11) https://doi.org/10.1029/92jb01059, 15425.

Rowland, J.V., Sibson, R.H., 2004. Structural controls on hydrothermal flow in a segmented rift system, Taupo volcanic zone, New Zealand. Geofluids 4 (4), 259–283. https://doi.org/10.1111/j.1468-8123.2004.00091.x.

Rutter, E.H., Holdsworth, R.E., Knipe, R.J., 2001. The nature and significance of fault zone weakening: an introduction. In: Holdsworth, R.E., Strachan, R.A., Magloughlin, J.F., Knipe, R.J. (Eds.), The Nature and Tectonic Significance of Fault Zone Weakening, vol. 186. Geological Society, London, Special Publications, pp. 1–11.

Sagy, A., Brodsky, E.E., 2009. Geometric and rheological asperities in an exposed fault zone. J. Geophys. Res. 114 (B2) https://doi.org/10.1029/2008jb005701.

Savage, H.M., Brodsky, E.E., 2011. Collateral damage: evolution with displacement of fracture distribution and secondary fault strands in fault damage zones. Journal of Geophysical Research - Solid Earth 116 (B3). https://doi.org/10.1029/2010JB007665.

Scholz, C.H., 1987. Wear and gouge formation in brittle faulting. Geology 15, 493–495. https://doi.org/10.1130/0091-7613(1987)15<493:WAGFIB>2.0.CO;2.

Schulz, S.E., Evans, J.P., 1998. Spatial variability in microscopic deformation and composition of the Punchbowl fault, southern California: implications for mechanisms, fluid–rock interaction, and fault morphology. Tectonophysics 295, 223–244.

Schwering, P.C., 2013. Geophysical Modeling of the Dixie Meadows Geothermal Prospect: Dual Analysis of Gravity and Magnetic Data towards Identifying Structural Controls. (MS). University of Nevada, Reno.

Scibek, J., Gleeson, T., McKenzie, J.M., 2016. The biases and trends in fault zone hydrogeology conceptual models: global compilation and categorical data analysis. Geofluids 16 (4), 782–798. https://doi.org/10.1111/gfl.12188.

Seront, B., Wong, T.-F., Caine, J.S., Forster, C.B., Bruhn, R.L., Fredrich, J.T., 1998. Laboratory characterization of hydromechanical properties of a seismogenic normal fault system. J. Struct. Geol. 20 (7), 865–881. https://doi.org/10.1016/S0191-8141(98)00023-6.

Shipton, Z.K., Cowie, P.A., 2001. Damage zone and slip-surface evolution over mm to km scales in high-porosity Navajo sandstone, Utah. J. Struct. Geol. 23, 1825–1844. https://doi.org/10.1016/S0191-8141(01)00035-9.

Shipton, Z.K., Roberts, J.J., Comrie, E.L., Kremer, Y., Lunn, R.J., Caine, J.S., 2019. Fault Fictions: Systematic Biases in the Conceptualization of Fault-Zone Architecture. Geological Society. Special Publications, London. https://doi.org/10.1144/sp496-2018-161.

Sibson, R.H., 1977. Fault rocks and fault mechanisms. Journal of the Geological Society of London 133 (3), 191–213. https://doi.org/10.1144/gsjgs.133.3.0191.

Sibson, R.H., 1987. Earthquake rupturing as a mineralizing agent in hydrothermal systems. Geology 15 (8), 701–704. https://doi.org/10.1130/0091-7613(1987)15<701:ERAAMA>2.0.CO;2.

Sibson, R.H., 2020. Preparation zones for large crustal earthquakes consequent on fault-valve action. Earth Planets Space 72 (1). https://doi.org/10.1186/s40623-020-01153-x.

Sibson, R.H., Robert, F., Poulsen, K.H., 1988. High-angle reverse faults, fluid-pressure cycling, and mesothermal gold-quartz deposits. Geology 16, 551–555. https://doi.org/10.1130/0091-7613(1988)016<0551:HARFFP>2.3.CO;2.

Simmons, S.F., White, N.C., John, D.A., 2005. Geological characteristics of epithermal precious and base metal deposits. Economic Geology 100th Anniversary Volume 485–522. https://doi.org/10.5382/AV100.16.

Sleep, N.H., Blanpied, M.L., 1992. Creep, compaction and the weak rheology of major faults. Nature 359, 687–692. https://doi.org/10.1038/359687a0.

Solum, J.G., Davatzes, N.C., Lockner, D.A., 2010. Fault-related clay authigenesis along the Moab Fault; implications for calculations of fault rock composition and mechanical and hydrologic fault zone properties. J. Struct. Geol. 32 (12), 1899–1911. https://doi.org/10.1016/j.jsg.2010.07.009.

Sosio De Rosa, S., Shipton, Z.K., Lunn, R.J., Kremer, Y., Murray, T., 2018. Along-strike fault core thickness variations of a fault in poorly lithified sediments, Miri (Malaysia). J. Struct. Geol. 116, 189–206. https://doi.org/10.1016/j.jsg.2018.08.012.

Speed, R.C., 1976. Geologic Map of the Humboldt Lopolith and Surrounding Terrane, Nevada. Geological Society of America.

Spörli, K.B., Cargill, H., 2011. Structural evolution of a world-class epithermal orebody: the Martha Hill Deposit, New Zealand. Society of Economic Geologists 106 (6). https://doi.org/10.2113/econgeo.106.6.975, 975-998.

Sutherland, R., Toy, V.G., Townend, J., Cox, S.C., Eccles, J.D., Faulkner, D.R., et al., 2012. Drilling reveals fluid control on architecture and rupture of the Alpine fault, New Zealand. Geology 40 (12), 1143–1146. https://doi.org/10.1130/g33614.1.

Swanson, M.T., 1989. Sidewall ripouts in strike-slip faults. J. Struct. Geol. 11 (8) https://doi.org/10.1016/0191-8141(89)90045-X, 993-948.

Swanson, M.T., 2005. Geometry and kinematics of adhesive wear in brittle strike-slip fault zones. J. Struct. Geol. 27 (5), 871–887. https://doi.org/10.1016/j.jsg.2004.11.009.

Tenthorey, E., Cox, S.F., Todd, H.F., 2003. Evolution of strength recovery and permeability during fluid-rock reaction in experimental fault zones. Earth Planet Sci. Lett. 206, 161–172. https://doi.org/10.1016/S0012-821X(02)01082-8.

Thompson, G.A., Burke, D.B., 1973. Rate and direction of spreading in Dixie Valley, Basin and Range Province, Nevada. Geol. Soc. Am. Bull. 84 (2), 627–632. https://doi.org/10.1130/0016-7606(1973)84<627:radosi>2.0.co;2.

Thompson, G.A., Meister, L.J., Herring, A.T., Smith, T.E., Burke, D.B., Kovach, R.L., Burford, R.O., Salehi, I.A., Wood, M.D., 1967. Geophysical study of Basin-Range structure,Dixie Valley region, Nevada. Air Force Cambridge Research Laboratory. Report No. 66-848.

Toy, V.G., Boulton, C.J., Sutherland, R., Townend, J., Norris, R.J., Little, T.A., et al., 2015. Fault rock lithologies and architecture of the central Alpine fault, New Zealand, revealed by DFDP-1 drilling. Lithosphere 7 (2), 155–173. https://doi.org/10.1130/l395.1.

Vanderburg, W.O., 1940. Reconnaissance of Mining Districts in Churchill County, Nevada, vol. 7093. United States Department of the Interior, Information Circular, IC, 57.

Vikre, P.G., 1993. Gold mineralization and fault evolution at the Dixie Comstock mine, churchill county, Nevada. Econ. Geol. 89 (4), 707–719. https://doi.org/10.2113/gsecongeo.89.4.707.

Wallace, R.E., Whitney, R.A., 1984. Late Quaternary history of the Stillwater Seismic Gap, Nevada. Bull. Seismol. Soc. Am. 74 (1), 301–314.

Watterson, J., Childs, C., Walsh, J.J., 1998. Widening of fault zones by erosion of asperities. Geology 26, 71–74. https://doi.org/10.1130/0091-7613(1998)026<0071:WOFZBE>2.3.CO;2.

Whitten, C.A., 1957. Geodetic measurements in the Dixie Valley area. Bull. Seismol. Soc. Am. 47 (4), 321–325.

Wibberley, C.A.J., Yielding, G., Di Toro, G., 2008. Recent advances in the understanding of fault zone internal structure: a review. Geological Society, London, Special Publications 299 (1), 5–33. https://doi.org/10.1144/sp299.2.

Wilden, R., Speed, R.C., 1974. Open-File Report 68-329: Geology and Mineral Deposits of Churchill County, Nevada. USGS.

Williams, R.T., Goodwin, L.B., Mozley, P.S., 2017. Diagenetic controls on the evolution of fault-zone architecture and permeability structure: implications for episodicity of fault-zone fluid transport in extensional basins. Geol. Soc. Am. Bull. 129 (3–4), 464–478. https://doi.org/10.1130/b31443.1.

Wilson, J.E., Chester, J.S., Chester, F.M., 2003. Microfracture analysis of fault growth and wear processes, Punchbowl Fault, San Andreas system, California. J. Struct. Geol. 25, 1855–1873. https://doi.org/10.1016/S0191-8141(03)00036-1.

Wintsch, R.P., Christoffersen, R., Kronenberg, A.K., 1995. Fluid-rock reaction weakening of fault zones. J. Geophys. Res.: Solid Earth 100 (B7), 13021–13032. https://doi.org/10.1029/94jb02622.

Woodcock, N.H., Dickson, J.A.D., Tarasewicz, J.P.T., 2007. Transient permeability and reseal hardening in fault zones: evidence from dilation breccia textures. Geological Society, London, Special Publications 270 (1), 43–53. https://doi.org/10.1144/gsl.sp.2007.270.01.03.

Woodcock, N.H., Mort, K., 2008. Classification of fault breccias and related fault rocks. Geol. Mag. 145 (3) https://doi.org/10.1017/s0016756808004883.

Yang, L., Zhao, R., Wang, Q., Liu, X., Carranza, E.J.M., 2018. Fault geometry and fluid-rock reaction: combined controls on mineralization in the Xinli gold deposit, Jiaodong Peninsula, China. J. Struct. Geol. 111, 14–26. https://doi.org/10.1016/j.jsg.2018.03.009.

Yasuhara, H., 2005. Fault zone restrengthening and frictional healing: the role of pressure solution. J. Geophys. Res. 110 (B6) https://doi.org/10.1029/2004jb003327.

Zhang, P., Mao, F., Slemmons, D.B., 1999. Rupture terminations and size of segment boundaries from historical earthquake ruptures in the Basin and Range Province. Tectonophysics 308, 37–52.

Zhang, P., Slemmons, D.B., Mao, F., 1991. Geometric pattern, rupture termination and fault segmentation of the Dixie Valley-Pleasant Valley active normal fault system, Nevada, U.S.A. J. Struct. Geol. 13 (2), 165–176. https://doi.org/10.1016/0191-8141(91)90064-.

Zoback, M.L., Anderson, R.E., Thompson, G.A., 1981. Cainozoic evolution of the state of stress and style of tectonism of the Basin and Range Province of the Western United States. Philos. Trans. R. Soc. London, Ser. A 300 (1545), 407–434. https://doi.org/10.1098/rsta.1981.0073.